Int J Appl Earth Obs Geoinformation 87 (2020) 102028

Contents lists available at ScienceDirect

Int J Appl Earth Obs Geoinformation

journal homepage: www.elsevier.com/locate/jag

Satellite interferometric data for landslide intensity evaluation in mountainous regions

Lorenzo Solari[a,*], Silvia Bianchini[b], Rachele Franceschini[b], Anna Barra[a], Oriol Monserrat[a], Patrick Thuegaz[c], Davide Bertolo[c], Michele Crosetto[a], Filippo Catani[b]

[a] Centre Tecnològic de Telecomunicacions de Catalunya (CTTC/CERCA), Geomatics Division, 08860, Castelldefels, Spain
[b] University of Firenze, Department of Earth Sciences. Via Giorgio La Pira 4, 50121, Firenze, Italy
[c] Regione Autonoma Valle d'Aosta, Assessorato Opere pubbliche, Difesa del suolo e edilizia residenziale pubblica. Loc. Amérique, 11020, Quart, Italy

ARTICLE INFO

Keywords:
Satellite interferometry
Landslide intensity
Potential loss
Mountainous region

ABSTRACT

Multi-Temporal Interferometric Synthetic Aperture Radar (MTInSAR) data offer a valuable support to landslide mapping and to landslide activity estimation in mountain environments, where in situ measures are sometimes difficult to gather. Nowadays, the interferometric approach is more and more used for wide-areas analysis, providing useful information for risk management actors but at the same time requiring a lot of efforts to correctly interpret what satellite data are telling us. In this context, hot-spot-like analyses that select and highlight the fastest moving areas in a region of interest, are a good operative solution for reducing the time needed to inspect a whole interferometric dataset composed by thousands or millions of points. In this work, we go beyond the concept of MTInSAR data as simple mapping tools by proposing an approach whose final goal is the quantification of the potential loss experienced by an element at risk hit by a potential landslide. To do so, it is mandatory to evaluate landslide intensity. Here, we estimate intensity using Active Deformation Areas (ADA) extracted from Sentinel-1 MTInSAR data. Depending on the localization of each ADA with respect to the urban areas, intensity is derived in two different ways. Once exposure and vulnerability of the elements at risk are estimated, the potential loss due to a landslide of a given intensity is calculated. We tested our methodology in the Eastern Valle d'Aosta (north-western Italy), along four lateral valleys of the Dora Baltea Valley. This territory is characterized by steep slopes and by numerous active and dormant landslides. The goal of this work is to develop a regional scale methodology based on satellite radar interferometry to assess the potential impact of landslides on the urban fabric.

1. Introduction

Considering the increasing socio-economic impacts of landslides worldwide, mainly due to the growth of urban settlements in landslide-prone areas (Petley et al., 2005), several methods and guidelines have been proposed for qualitative and/or quantitative landslide risk estimation. Risk has been investigated as a general framework or as for single components, such as intensity, vulnerability or exposure (i.e. Dai et al., 2002; Ko et al., 2004; Glade et al., 2006; Corominas et al., 2014). These parameters can be evaluated in different ways, depending on the input data quality and on the working scale; a unique way to derive them cannot be found in literature (Fell et al., 2008).

Landslide risk is particularly difficult to assess over wide areas because detailed information about landslide occurrence, spatial and temporal probability, runout modelling, vulnerability and exposure assessment is usually quite challenging to derive (Van Westen et al., 2006; Strozzi et al., 2013). At regional to medium scale (1:250,000 – 1:25,000) landslide risk products are used for urban planning activities and to define long-term strategies for risk reduction (Corominas et al., 2014).

Vulnerability is generally defined as the degree of loss of a given element at risk to the occurrence of a landslide of given magnitude. It is related to the amount of damage the exposed elements at risk could suffer due to a certain hazard (Winter et al., 2014). It is a difficult parameter to estimate if detailed damage data are not available and because landslide magnitude cannot be easily foreseen (Van Westen

* Corresponding author at: Centre Tecnològic de Telecomunicacions de Catalunya (CTTC/CERCA), Geomatics Division, 08860, Castelldefels, Spain.
E-mail addresses: lorenzo.solari@cttc.cat (L. Solari), silvia.bianchini@unifi.it (S. Bianchini), rachele.franceschini@stud.unifi.it (R. Franceschini), anna.barra@cttc.cat (A. Barra), oriol.monserrat@cttc.cat (O. Monserrat), p.thuegaz@regione.vda.it (P. Thuegaz), d.bertolo@regione.vda.it (D. Bertolo), michele.crosetto@cttc.cat (M. Crosetto), filippo.catani@unifi.it (F. Catani).

https://doi.org/10.1016/j.jag.2019.102028
Received 10 July 2019; Received in revised form 31 October 2019; Accepted 2 December 2019

et al., 2006). Vulnerability is a concept that can be applied to people or buildings/infrastructures (in this case is known as "physical vulnerability"). Considering the large and intrinsic uncertainties, the degree of loss of human life is rarely assessed. Some authors proposed solutions based on population census data or consequence analysis (Bell and Glade, 2004). Physical vulnerability has been more widely used in landslide studies, still requiring some information about building/infrastructure typology or potential damage degree. Usually, physical vulnerability is expressed by a relative scale ranging from 0 (no damage) to 1 (complete damage) and can be estimated using heuristic methods (e.g. Winter et al., 2014), data driven methods (the most frequently used, e.g. Kaynia et al., 2008) or analytical methods (less frequently implemented because of their complexity, e.g. Mavrouli and Corominas, 2010).

Exposure is assumed to be a characteristic of the element at risk (person or structure) and it is referred to its location and economic value (Glade et al., 2006). Population exposure requires specific studies aimed to evaluate the day/night fluctuation of exposed people. It depends on building use as well (e.g. Schwendtner et al., 2013). Building exposure essentially depends on the type of element at risk considering the interaction between the structure and a given event under a constant level of risk (Glade et al., 2006).

Landslide intensity is a crucial parameter to be defined for a correct evaluation of vulnerability and of the expected degree of loss. As defined by Hungr (1997), intensity is an evaluation of landslide destructiveness. It is related to the type of landslide, its propagation mechanism and volume. Intensity is a highly site-dependent, non-straightforward task for which no standardized methodology exists (Uzielli et al., 2008). Cardinali et al. (2002) proposed a landslide intensity classification based on two parameters: volume and velocity of the phenomenon. Lateltin et al. (2005) presented an overview about risk management in Switzerland, reporting that landslide intensity is related to different parameters, depending on the type of event (such as thickness and velocity of the mass for debris flows). Jakob (2005) demonstrated how debris flows intensity is closely related to their size, in terms of volume, peak discharge and inundated area. Therefore, the estimation of intensity classically relies on landslide models or empirical formulas aimed at calculating landslides volume.

Nowadays, it is possible to assess intensity by means of earth observation products such as Multi-temporal Interferometric Synthetic Aperture Radar (MTInSAR) data. These earth observation products can help defining the magnitude of potential slow-moving landslides, parameter useful for landslide intensity (Guzzetti et al., 2006). MTInSAR data have been used by some authors for this kind of evaluation. For example, Cigna et al. (2013) exploited MTInSAR products for landslide state of activity and intensity appraisal by means of an "activity matrix" whose inputs where interferometric-derived ground velocity information. This approach has been followed by Oliveira et al. (2015) to assess the potential of MTInSAR data for new landslide definition in the Grande da Pipa River basin (Portugal). Bianchini et al. (2017b) presented a GIS-based (Geographical Information System) procedure aimed to evaluate specific risk in a hilly municipality of Tuscany Region (central Italy). Interferometric products were used as landslide intensity zonation tools.

In a more general framework, MTInSAR data have a high potential to provide useful information about "new" landslides, highlighting unknown phenomena that have not been previously mapped. The effectiveness of MTInSAR data have been especially proven in mountain environments, where in situ information are difficult to obtain, especially by hotspot approaches (Hölbling et al., 2012; Liu et al., 2013; Del Ventisette et al., 2014; Raspini et al., 2016; Bianchini et al., 2012, 2017a; Imaizumi et al., 2018; Lu et al., 2019; Solari et al., 2019).

In this work, we go beyond the concept of MTInSAR data as mapping tools by proposing a simple and reproducible work flow which has as starting point a deformation map derived from satellite radar data. The deformation map is analyzed to automatically extract the fastest moving areas (Active Deformation Areas – ADA) with common Persistent Scatterers (PS) behavior. The ADA extraction methodology was newly conceived and developed in Barra et al. (2017) and already used in some recent literature (Pastonchi et al., 2018; Solari et al., 2018; Tomás et al., 2019). The ADA are the first product of the chain, whose final goal is to quantify the potential loss (by an economic point of view) suffered by a building or road if the motion persists or accelerates. The methodology aims to derive landslide intensity using the ADA in a dual form: as direct estimation of landslide magnitude (and intensity) and as an indicator for the presence of unstable debris covers that could be the source areas of future debris flows, whose runout is foreseen by means of a basin scale model. The methodology has been tested in Eastern Valle d'Aosta (north-western Italy) along four lateral valleys of the Dora Baltea Valley in a territory characterized by steep slopes and widespread active and dormant landslides. Palomba et al. (2015) reported that from 1984 the number of landslide events above 2000 m a.s.l. may have slightly increased, highlighting the need for remotely sensed motion data in partially or totally inaccessible areas.

The methodology has been conceived in the framework of the "U-Geohaz - Geohazard impact assessment for urban areas" project, co-funded by the European Commission, Directorate-General Humanitarian Aid and Civil Protection (ECHO). The main goal of the project is to develop a methodology based on Sentinel-1 radar images to continuously assess the potential impact of geohazards on urban areas and critical infrastructures.

2. Study area

The test area of our methodology is eastern Valle d'Aosta (VdA), an alpine region in north-western Italy. The area of interest is mainly mountainous with peaks reaching 4000 m a.s.l. and it is characterized by a main East-West valley, where the Dora Baltea flows, and by five tributary valleys (from west to east: Valpelline, Saint Bartelemy, Valtournenche, Ayas and Gressoney valleys - Fig. 1).

The current landscape has been highly influenced and controlled by the glacial action and by the tectonic/geodynamic evolution of VdA (Martinotti et al., 2011). The latter reflects the complex collision between the European and Adria plates that created an imbricated pile of metamorphic continental and oceanic domains (Polino et al., 1990). These tectono-metamorphic units were later affected by neotectonic faulting, i.e. along the Aosta-Ranzola fault that crosses the eastern part of the Dora Baltea valley (Bistacchi et al., 2001). This post collisional activity influences the relief evolution and the current slope dynamics due to the inherited geo-structural and tectonic settings (Carraro and Giardino, 2004). After the last glaciation maximum, the action of ice concurred in modelling the landscape of VdA, configuring the current valleys orography, leaving erosional or depositional landforms and directly influencing mass wasting processes due to debuttressing (Carraro and Giardino, 2004).

Land cover is dominated by forests and grasslands below 2000 m a.s.l., gradually replaced above this altitude by debris, sparse vegetation and bare rock. At the highest altitudes few perennial glaciers are still present. Urban areas can be found only along valley bottoms and overall below 1500 m a.s.l.; large valley sectors are considered inhabited.

Climate is highly influenced by altitude and it is characterized by precipitation regimes of 1000 – 1110 mm/year in the tributary valleys and of 600 mm/year in the Dora Baltea Valley (Ratto et al., 2003). During winters, snowfalls are frequent. Extreme rainfall events are common between late spring (end of April – May) and early autumn (September – beginning of October), registering cumulated rainfalls higher than 250 mm in few days (Salvatici et al., 2018).

The area of interest is characterized by 972 mapped landslides, included in the IFFI (Inventario dei Fenomeni Franosi in Italia – Italian landslide inventory, Trigila et al., 2010) catalogue of the region (Fig. 2). Different types of landslide are well represented in eastern VdA, ranging

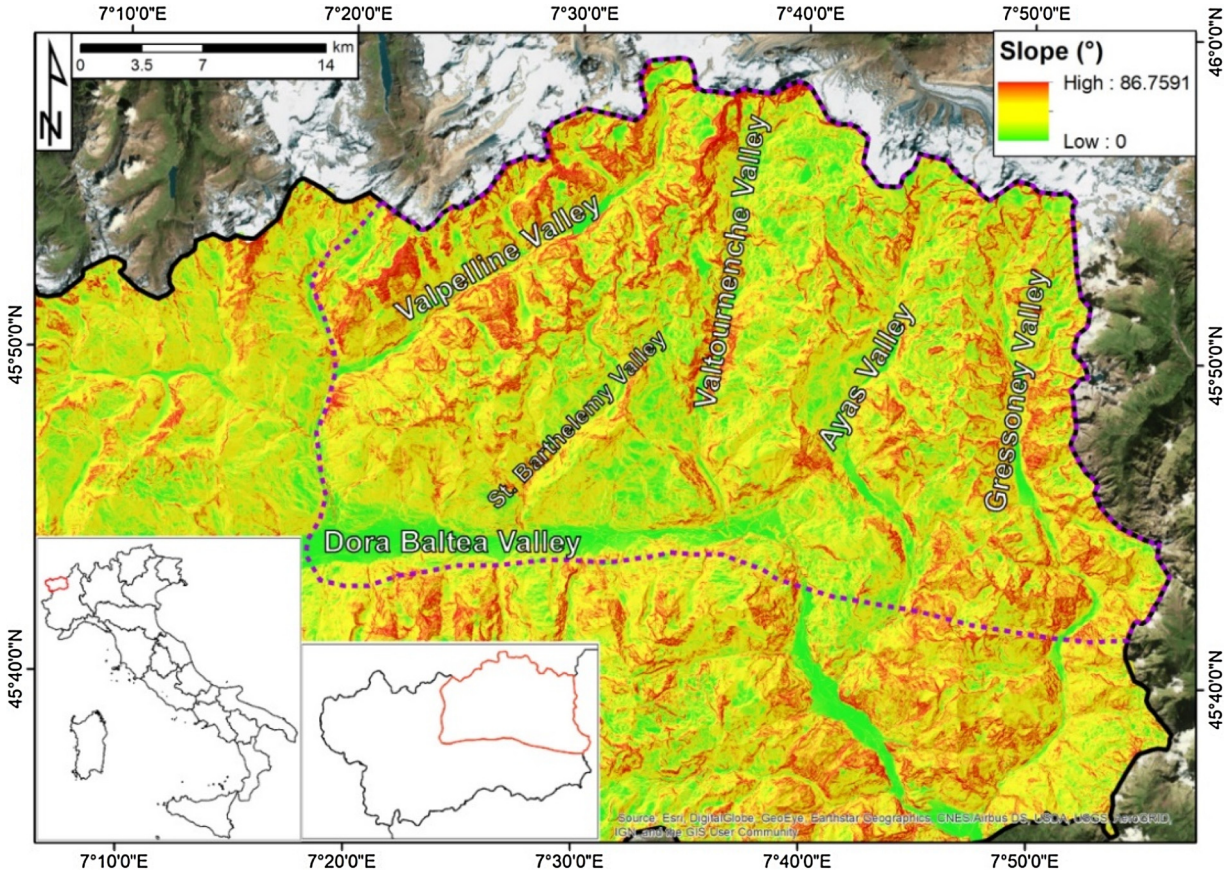

Fig. 1. Slope map of the area of interest derived from a 10 m Digital Elevation Model (DEM). The background image is an ESRI World Imagery orthophoto.

between very slow and slow-moving phenomena (DSGSD - Deep-Seated Gravitational Slope Deformation, rotational and complex landslides) to fast-moving landslides, such as debris and mud flows. Considering the areal extent of landslides, the most representative type is DSGSD which alone covers 152 km^2, with single mapped phenomena covering more than 10 km^2. The landslide index of this area (ratio between the area covered by landslides and the whole territory) is equal to 20 %, consistent with the regional value (18 %, Solari et al., 2019). In the area of interest, landslides are a major threat, causing high economic losses (both direct and indirect) and in some cases casualties, such as in October 2000 when a series of debris flows severely hit this sector of VdA, killing 17 people (Ratto et al., 2003).

3. Methodology

The methodology aims to derive vulnerability and potential loss maps starting from a regional scale deformation map obtained through MTInSAR analysis, which is the main input (Fig. 3). Because of the morphological context, landslides are our target; the methodology can be anyway adapted to other geohazards.

The first product to be derived is the ADA database which contains all the moving areas detected in the area of interest, following the approach proposed by Barra et al. (2017). Depending on the localization of each ADA, landslide intensity is defined in a twofold manner:

1) "ADA-related intensity". Landslide intensity depends on the average velocity of the ADA. This approach is applied only when a moving area directly overlaps one or more buildings/roads or an urban area ("Urban area – YES" condition in the workflow of Fig. 3);
2) "Model-related intensity". Landslide intensity depends on the run out of a potential landslide that could be originated from a debris-covered area showing high deformation rates and highlighted as ADA. We define as "debris" every type of slope or colluvial deposits containing blocks and more fine-grained materials and originated by slope dynamics (e.g. rockfalls deposits). The landslide run-out could hit one or more buildings/roads. This approach is applicable when a moving area is found outside of an urban area ("Urban area – NO" condition in Fig. 3) and in correspondence of a potential source of debris flows ("Geo-indicators – YES" condition in Fig. 3).

The geo-indicators are defined using a qualitative approach based on a preliminary analysis of all the ancillary data available. Topographic maps and DEMs (and DEM-derived products – slope and aspect) are used for the delineation of the geomorphological characteristics of a slope (e.g. curvature, presence of trenches or channels, water shed). Orthophoto, geological maps and ground data (when available) are used to estimate the presence of debris deposits (as previously defined).

If an ADA does not fall into one of the two limiting conditions of the workflow, the approach cannot be applied.

Once the landslide intensity is calculated, exposure of the elements at risk and vulnerability are defined. Exposure evaluation is performed on a cadastral polygonal database of buildings and roads which is reclassified on the basis of the presumed asset value. Vulnerability is expressed as the degree of potential loss (ranging from 0 to 1) with respect to a given intensity (Fell et al., 2008). The potential loss is calculated as product between vulnerability and exposure considering a certain level of intensity and it is estimated as a monetary value. These concepts are developed later in this document.

The final products are two. A database of elements at risk indicating, in addition to the type of structure and its exposure, the value of vulnerability and potential loss for an event of given intensity (as defined in Fig. 3). Color coded maps of vulnerability and potential loss for each case study in which the methodology has been applied.

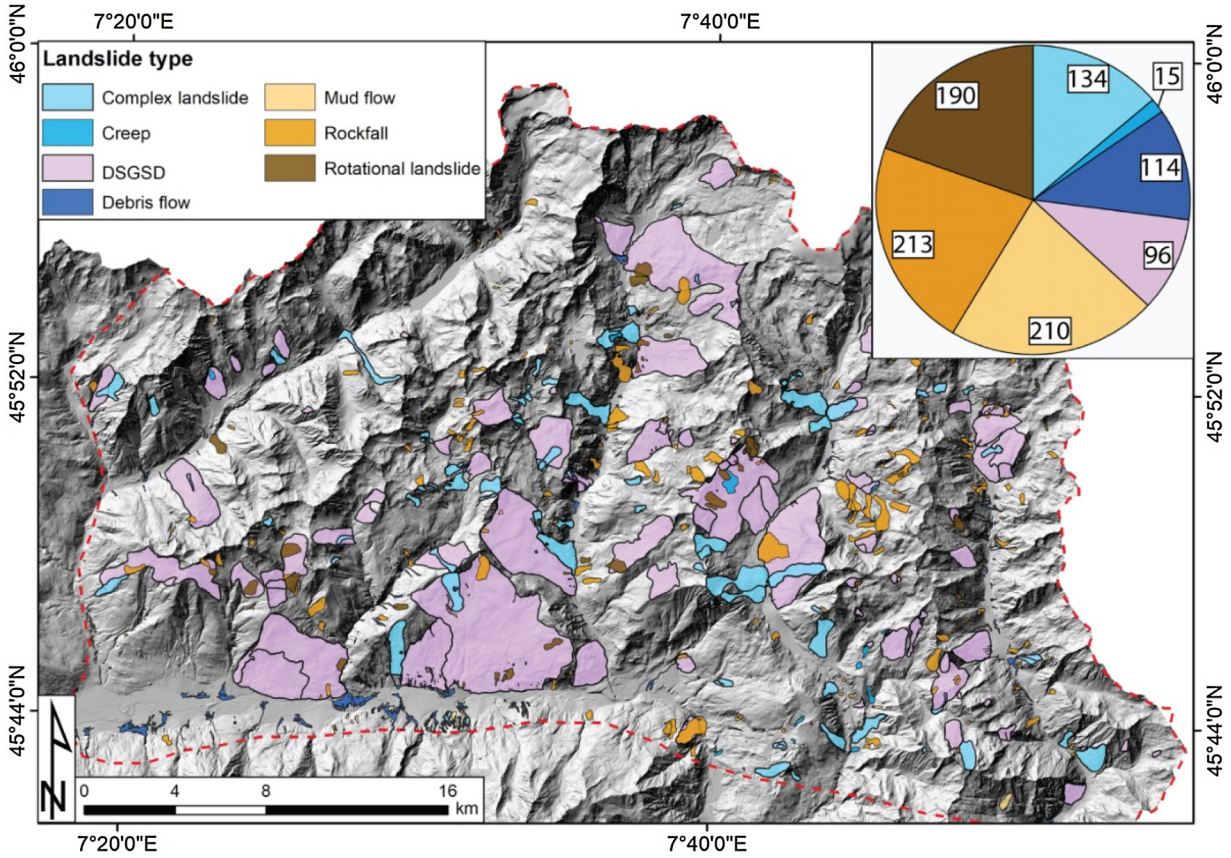

Fig. 2. Landslides distribution extracted from the IFFI catalogue of the Valle d'Aosta Region. The colors of the pie chart are referred to the map legend. The background image is a hillshade derived from a 10 × 10 m DEM.

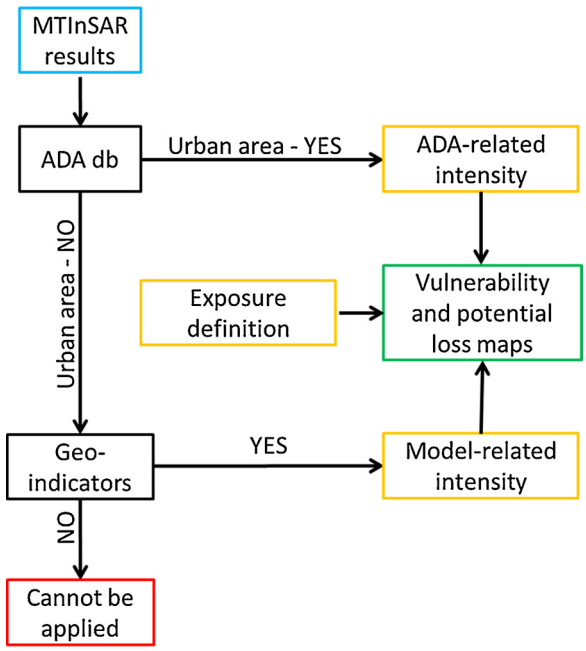

Fig. 3. Workflow of the methodology. MTInSAR, Multi-Temporal Interferometry; ADA, Active Deformation Areas; db, database.

In the following sections each phase of the workflow will be described, starting from the generation of the deformation map.

3.1. Deformation map generation

In this work, a total of 153 Sentinel-1 images were analyzed by means of a specifically developed MTInSAR approach. Sentinel-1 images are acquired in C-band (wavelength 5.55 cm) with a revisiting time of 6 days considering both satellites (1A and 1B) and a ground resolution of 14 by 4 m. The radar images cover the period January 2015 – August 2018 and have been acquired in descending orbit with VV polarization; the area of interest is covered by 2 bursts and 2 swaths. The incidence angle of the electromagnetic wave is on average equal to 38.7°. The low temporal baseline granted by Sentinel-1 allows reducing temporal decorrelation effects in the interferometric pairs and increasing the number of coherent pixels (Hanssen, 2001).

The MTInSAR strategy used here is subdivided into 3 phases aimed to generate the final deformation map: 1) generation of interferograms and coherence maps, 2) estimation of the annual linear velocity along the LOS (Line Of Sight) and 3) generation of deformation time series. We will now introduce the key steps of this interferometric chain and we refer to Devanthéry et al. (2014) and Barra et al. (2017) for further technical details.

Interferograms are generated with a maximum temporal baseline of 600 days at full (20 × 4 m) resolution. The related coherence maps were derived using a 2 × 10 multi-looked resolution (40 × 40 m). The whole interferometric stack is composed of 4012 interferograms that will be selected for further analyses depending on their temporal baseline and coherence. This latter parameter is of great importance in a mountain region such as VdA where coherence is particularly affected by seasonal variations because of snow cover (Kumar and

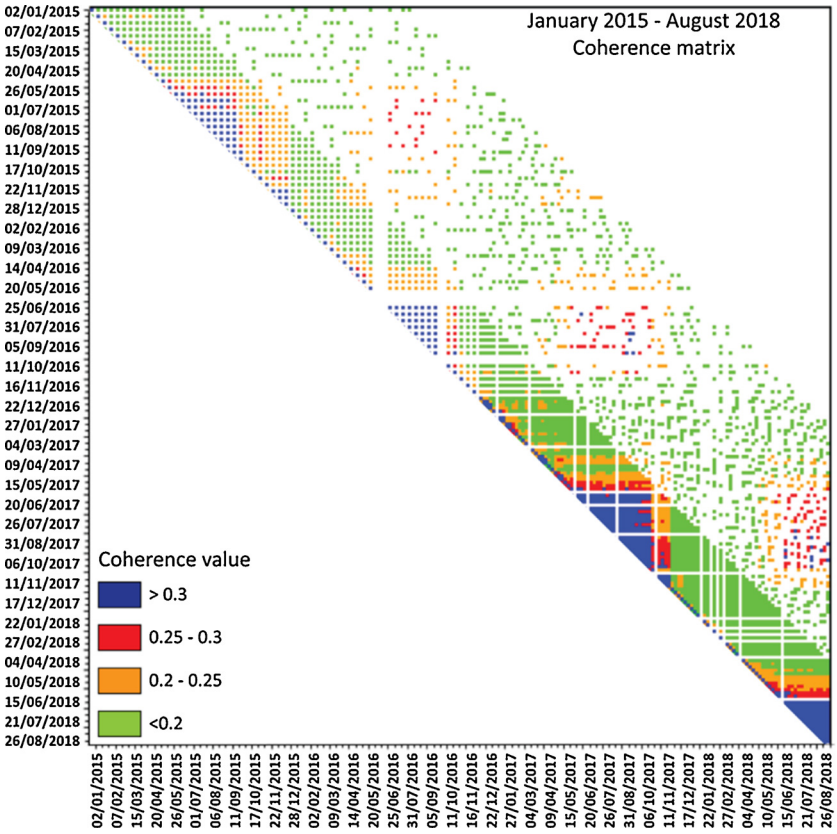

Fig. 4. Coherence matrix generated for the interferometric stack. The absence of an interferogram is due to the unavailability of one of the two required images or because the maximum temporal baseline (600 days) has been reached. The higher density of interferograms in the right lower corner is due to the increase of the revisiting time of Sentinel-1 constellation from 6 to 12 days.

Venkataraman, 2011). For this reason, a Coherence Matrix (CM) is adopted to study the temporal variation of coherence of the whole interferometric stack (Fig. 4). The CM is an asymmetric diagram showing the calculated mean coherence value over a selected area for each master-slave pair. The diagonal of the matrix represents the theoretical interferograms with temporal baseline equal to zero. By moving away from the diagonal, the temporal baseline increases with 6 days steps.

To remove the topographic contribution from the interferograms, we have used the 90 m resolution Shuttle Radar Topographic Mission (SRTM) Digital Elevation Model provided by NASA (National Aeronautics and Space Administration), and the precise orbits provided by the European Space Agency (ESA). The resolution of the DEM is enough to properly remove the topographical component from the interferogram network and calculate the residual topographic error.

The CM is useful to highlight that coherence is on average low (only few interferograms with values higher than 0.35) and characterized by a clear seasonal oscillation. From May to November interferograms are generally more coherent than interferograms generated with images acquired between December and April, when coherence is always below 0.25. This means that not only coherence of 6-days interferogram is higher in summer but also that in some cases a winter 6-days interferogram has lower coherence than a one-year interferogram between two summer seasons.

Thanks to the CM is possible to select the best combination of interferograms for extracting ground deformation data. For the velocity estimation, the network is composed of 432 interferograms with minimum temporal baseline of 150 days and minimum average coherence of 0.2. For the time series generation, the network is composed of 1325 interferograms with low temporal baselines (up to 6 days) and minimum average coherence of 0.2.

Several statistical criteria have been presented to discriminate between noisy and coherent pixels (for a literature review we refer to Crosetto et al., 2016). In this work, the first selection of pixels is based on the Dispersion of Amplitude (DA, Hanssen, 2001); the DA threshold here used is equal to 0.4. The best-fitting linear model of velocity is estimated for these points. A second selection of pixels relies on the gamma threshold, which quantifies the residuals between the model and the observations, i.e. the level of fitting between the linear model and the observations (Biescas et al., 2007; Devanthéry et al., 2014). Since the deformation model is linear, a restrictive gamma threshold can cause the non-selection of the points with a non-linear movement. Here the gamma threshold is fixed to 0.37, which resulted to be the best trade-off between low noise level and spatial density of pixels for the whole study area.

Annual velocities are calculated following the approach proposed by Biescas et al. (2007) and Crosetto et al. (2011). Time series estimation is based on a two-step phase unwrapping process. In the first step each interferogram is spatially unwrapped using the Minimum Cost Flow method (Costantini et al., 1999). In the second step the consistency of the spatial unwrapping is evaluated in time and on a pixel-wise basis (Devanthéry et al., 2014). The non-linear component of deformation is estimated and included in the time series. To decrease the aliasing errors, it is important to have a spatial continuous sampling of PS and a low temporal baseline of interferograms. The redundancy of the observations is also crucial to detect and correct possible aliasing errors (a minimum of 5 interferogram for each image is required).

3.2. ADA database generation

The concept of "Active Deformation Area - ADA" has been developed by Barra et al. (2017) and adapted by Solari et al. (2018) for Civil Protection purposes. An ADA is composed by spatially aggregated moving points above a selected velocity threshold. The cluster is defined depending on parameters such as the minimum number of PS that an ADA must contain, or the clustering radius built around every moving PS. Each PS is characterized by a quality index which estimates the spatial and temporal correlation between all the time series of each PS composing an ADA. A high quality index means that time series are

well correlated, and thus a more reliable information about the phenomenon is detected. We refer to Barra et al. (2017) for an in-depth explanation of the ADA approach.

The procedure developed by Barra et al. (2017) has been automatized into a software, "ADA-finder" (Navarro et al., 2018; Tomás et al., 2019), which analyzes a large stack of PS points in just few seconds/minutes. The software is implemented in C++ and uses as input a ESRI shapefile of PS points with some mandatory fields such as geographic coordinates, velocity and displacement values. The user has to fix just a few input parameters before running the software:

- input/output files path;
- isolation distance, i.e. the minimum distance at which a point can be considered isolated from the others. Isolated points are not considered by the software and removed. This selection is implemented before the definition of the "moving points" to a priori exclude isolated PS. As demonstrated by the experience, these PS are probably not representative of a landslide but are more probably related to noise or single objects motion (Solari et al., 2018). We used a value of 100 m as isolation distance. The value is a good compromise between spatial resolution of the satellite and PS density;
- standard deviation factor (σ), i.e. the standard deviation value of the LOS deformation velocity of the PS population. The σ value represents a measure of the dispersion of the dataset and can be used to set the stability range of PS velocity. This value is used to define whether a PS is "moving" or not. Here we fixed a value equal to 2;
- clustering radius, i.e. the maximum distance at which a PS can be considered as part or not of a cluster. The clustering approach implemented in the software relies on a Depth First Search method (Horowitz and Sahni, 1976) to identify the connected components between PS points. The clustering radius is here equal to 28 m, i.e. two times the ground resolution of Sentinel-1. If the distance between two points is higher than the clustering radius, they will not be considered as part of the same cluster;
- minimum ADA size, i.e. the minimum number of PS points which an ADA must contain for being representative for a small landslide. Considering C-band satellites, the ideal number of PS points to detect a small landslide is five (Herrera et al., 2013).

The software's output is an ADA database containing two shapefiles: one polygonal for the clusters and one punctual for the PS included in every cluster. The ADA generated in this way are the main input for all the subsequent evaluations regarding landslide vulnerability and potential loss.

3.3. Landslide intensity evaluation

Each ADA can be used for landslide intensity assessment in two different ways: one as direct estimation of landslide magnitude (and thus intensity) and as an indicator for the presence of unstable debris deposits that could be the source areas of future debris flows, whose runout is foreseen by means of a basin scale model. The first approach is named as "ADA-related intensity", the second one as "Model-related intensity" (Fig. 3). Intensity is needed to derive vulnerability of the elements at risk and the potential loss as it will be explained in section 3.4 and 3.5. The first intensity approach is aimed to investigate in a direct way those landslides showing the highest deformation rates in VdA (complex or rotational). The second intensity approach is implemented to indirectly (using the ADA as source areas) derive information about potential debris flows.

3.3.1. ADA-related intensity

This approach has been inspired by the landslide activity matrix proposed by Cigna et al. (2013), in which intensity is a direct expression of landslide velocity (derived from LOS deformation rates of the interferometric products). Here, we do not use a "representative velocity" (Cigna et al., 2013) for each landslide but we rely on the ADA as indexes of slope movements. This approach has been already followed by Solari et al. (2018) for geohazards mapping in Canary Islands (Spain). Landslide intensity is defined by the average LOS velocity of the ADA, following the classification:

- intensity 1, average velocity lower than 16 mm/yr;
- intensity 2, average velocity ranging between 16 and 32 mm/yr;
- intensity 3, average velocity higher than 32 mm/yr.

The first threshold (16 mm/yr) is representative for the passage between extremely slow and very slow landslides, as assumed by Cruden and Varnes (1996). We derived the second one (32 mm/yr) by doubling up the first value.

The ADA-related method does not consider volume for determining landslide intensity. Although volume is an important component of intensity, its estimation over wide areas requires the definition of magnitude–frequency distributions based on long-term inventories and spatially distributed power law exponents (Catani et al., 2016). Considering these requirements, we think that velocity is enough to describe landslide intensity at the regional scale using a reproducible method and few ancillary inputs.

3.3.2. Model-related intensity

In the area of interest, the use of the ADA-related approach is limited. In fact, the urban density is quite low and just a part of the ADA respect the input condition ("Urban area – YES", Fig. 3). For this reason, a second approach (Model-related intensity) has been defined to maximize the information extracted from the satellite data.

If one ADA does not directly intersect elements at risk, further evaluations are made. In this case the presence or not of debris (following the concept previously introduced) discriminates between the possibility or not to apply this approach ("Geo-indicators – YES" condition in Fig. 3). It is based on the use of ADA as indicators of active mass wasting processes, especially involving unstable debris deposits of different origin that could be source areas for catastrophic debris flows. These types of events, usually triggered by extreme rainfalls, are the most damaging, in terms of economic and life loss, for the Valle d'Aosta Region (Ratto et al., 2003). If an ADA coincides with a debris-covered area, defined on the basis of geological and orthophoto information, a run-out model will be used to evaluate the possible landslide evolution, in terms of landslide path and spatial distribution of the accumulation zone. In this work, the Gravitational Process Path model (GPP, Wichmann et al., 2017) has been chosen to define the potential run-out of moving debris along slopes.

The GPP model is specifically designed to simulate the path and run-out area of gravitational processes, such as debris flows, avalanches and rockfalls, or snow avalanches. The model is suited for regional or basin scale analysis requiring only few and simple terrain parameters for the source area and a DEM of the slope. In brief, the GPP model simulates the motion of a mass point from a source to the deposition area through the use of different release, process path, run-out and deposition models. The modelling approaches are not entirely physically based but follow empirical principles simulating the main features of a mass moving along a slope (Wichmann et al., 2017). The simplest model configuration requires only a DEM and a contour of the potential source area to run; thus, it is the best operational solution for basin/regional scale investigations, where detailed geotechnical and hydrogeological parameters, inputs for physically based numerical simulations, cannot be gathered. The GPP model is implemented into the open source GIS SAGA (System for Automated Geoscientific Analyses, Conrad et al., 2015).

In this work, we used a 2 m DEM as input for the model. The source areas have been defined within each ADA and selected considering the distribution of moving points and the local morphology. If the material height (thickness) for each starting cell of the source area is given as

input data, the GPP model allows modelling both sink filling along path and deposition. In order to obtain the soil/debris thickness, we used the results derived within the area of interest by Salvatici et al. (2018) using the Geomorphologically Indexed Soil Thickness model (Catani et al., 2010).

The random walk model defines the process path of a single particle from the initiation area to the deposition area following multiple flow directions (Wichmann, 2017). Three model parameters must be set: 1) a terrain slope threshold defining when the flow diverges (equal to 40° in our case); 2) an exponent for divergent flow which controls how much the flows diverges (a high value determine a higher lateral spread, we set this parameter to 1.5) and 3) a persistence factor that expresses how much a flow direction is preserved accounting for the inertia of the flow (Takahashi et al., 1992). We set this parameter to 1.5. We used the two-parameter friction model developed by Perla et al. (1980) to simulate the run-out length of the starting particles. This model, originally developed for snow avalanches, has been later adapted for debris flows (Wichmann et al., 2009). It is a center-of-mass model in which two parameters which govern the motion of the particle must be defined: the sliding friction coefficient (μ) and the mass-to-drag ratio. The sliding friction coefficient decreases as the catchment area increases and it is calculated from the following empirical law (Gamma, 2000): $\mu = 0.19 * a^{-0.24}$, where a is the catchment area. The mass-to-drag ratio depends on the size distribution of the material. For debris flows made by granular materials and blocks is on average equal to 70, value adopted in this work (Zimmermann et al., 1997). Finally, for modelling the material deposition we exploited a slope and on stop approach (the mass starts to be deposited when a slope threshold is reached – Wichmann et al., 2017) in which the deposition of material starts when the slope falls below 15°. Considering the material availability (depending on the soil thickness layer), the model distributes the height of material for each iteration; if a sink is encountered, it is progressively filled at every new iteration. All values reported are referred to the two case studies that will be presented in the section 4.3.

In summary, once the ADA that fulfill the "Geo-indicators" condition are selected, they are firstly grouped for geomorphological macro-areas (at flank scale). Then, the GPP model is run to reconstruct the spatial development of a known debris flow in each macro-area to obtain the input parameters to be used for the new models (based on the ADA distribution). If this is not possible, one of the ADA in each macro-area has to be selected as test site for the GPP model. The derived input parameters are then transferred to other ADA-sources.

The outputs of the model are four: 1) process area, defining the transition frequencies at every cell; 2) deposition, equal to the height of the material deposited at each cell; 3) maximum velocity reached by the flow at every cell and 4) stopping position, i.e. all the cells where the run-out length is reached. In this work, we used the deposited height of material at every cell as a proxy for landslide intensity. The three intensity classes are:

- intensity 1, height of the material lower than 1.25 m;
- intensity 2, height of the material between 1.26 and 2 m;
- intensity 3, height of the material higher than 2.01 m.

The values chosen are defined following the vulnerability functions derived by Papathoma-Köhle et al. (2012) using real debris flow events in South Tyrol (Austria) and represent a degree of loss of 30 %, 60 % and higher than 60 %, respectively.

3.4. Vulnerability and exposure definition

A value of vulnerability and exposure is assigned to every building or road, depending on their typology and using a simple classification approach illustrated in Table 1. The building/road database derives from the 1:2000 cadastral map of the VdA region, from which the polygons/lines have been extracted.

Table 1
Vulnerability and exposure values for the area of interest. V, vulnerability; I, intensity; E, exposure. Range values of E refers to the average between minimum and maximum values among the 33 municipalities. Single value are valid for all the 35 municipalities.

Type of building/road	V (I = 1)	V (I = 2)	V (I = 3)	E (€/sqm)
Barn	0.2	0.4	0.6	80
Camping	0.4	0.6	0.8	2600
Greenhouse	0.2	0.4	0.6	50
Hotel	0.15	0.3	0.5	1550 – 4600
Industrial laboratory	0.1	0.2	0.5	740 – 1000
Local road	0.6	0.8	1	50
Motorway	0.4	0.6	0.8	350
Municipal road	0.6	0.8	1	150
Office/service sector	0.1	0.3	0.6	1175 – 2600
Private house	0.2	0.35	0.6	1075 – 4350
Provincial road	0.6	0.8	1	180
School complex	0.3	0.5	0.7	4000
Shed	0.2	0.4	0.6	540-890
Commercial building (shop, restaurant, etc…)	0.2	0.35	0.6	865 – 2100
Shopping mall	0.2	0.35	0.6	1400 – 2200
Sport facilities	0.3	0.5	0.7	15-120
Stable	0.15	0.4	0.6	120
Regional/State road	0.4	0.6	0.8	250
Warehouse	0.2	0.4	0.6	680 - 1000

One of the first frameworks for landslide hazard and risk mapping over wide areas was developed by Catani et al. (2005) for the Arno River basin. Considering our working scale on large area, we followed a similar method in which vulnerability varies between 0 (no damage) and 1 (complete loss) as a function of landslide intensity. Three vulnerability classes are used, corresponding to three damage levels: aesthetic, functional and structural. This subdivision has been firstly proposed by Cardinali et al. (2002) and it is classically used for qualitative vulnerability evaluation (Sterlacchini et al., 2014). Each value of vulnerability is defined by the typology of element at risk following a data driven approach and considering the possible interactions between elements and landslide. Linear elements have the highest vulnerability values for each intensity class. If intensity is equal to zero, then vulnerability is null.

Exposure is referred to the economic value of an object and is estimated separately in different ways for each building class. We decided to implement different sources of information (market and income value, construction cost, renovation cost) to provide a plausible value for every structure. This is the maximum level of detail we could reach when working at basin scale; further information regarding people occupancy and day/night activity cannot be collected at this scale in a reasonable time. Our approach well fits in the one proposed by Pellicani et al. (2014) for wide areas with small data availability. These authors derived for each municipality of an Apennine portion of Apulia region (southern Italy), the maximum, minimum and average economic values of 25 types of assets, including industries and agricultural terrains. For each municipality the maximum value is given by the market value (OMI database) and the minimum by the construction cost in euros/sqm or the agricultural unit in euros/hectare. More detailed approaches can be proposed when damage data connected to a single event are available. For example, Vranken et al. (2013) estimated both direct and indirect damage due to landslides in the Flanders (Belgium) using the repair and prevention costs for infrastructures and private houses. On one side, this approach allows having a more realistic value of exposure for each object. On the other side, it requires single events information which are not simple to collect over wide areas but are more connected to the activities of single municipalities.

VdA is a region mainly devoted to tourism and just few large industries are present. Considering this, an effort was made to properly define the value of private houses, potentially being rented by tourists, and, in general, of building related to the tertiary sector. In this work,

we did not consider the exposure of cultural heritages, due to the difficulties in defining a common range of values for all the different structures.

Exposure for private houses is determined by the market value, as defined in the OMI (Osservatorio del Mercato Immobiliare – Real estate market observatory) database. Every Italian municipality is subdivided by the Agency of Revenue into subzones with different market values depending on the location (city center, industrial area and so on) and on the building state. The database is open and available online (OMI database, 2018). This is a certified source of information coming directly from the Italian central government and it is based on real estate market information collected every year. This database has been already used by other researchers and it can be considered a reliable dataset for scientific usage. Peduto et al. (2018) exploited the OMI database as "most likely market value" for a quantitative analysis of masonry buildings response to landslide in a small town of Calabria (Southern Italy). This solution refers to the work of Lari et al. (2012) who calculated the minimum and maximum market value for each census parcel of the city of Brescia (northern Italy) to derive exposure to floods, earthquakes and industrial accidents. Considering these examples and our working scale, we believe that the use of OMI-derived market value is the right choice for those building categories contained into the OMI catalogue (private houses, commercial buildings, offices, sheds). It is in fact the most detailed information we can gather at regional scale without the need of on field information sometimes impossible to obtain in short times and with low human efforts. This is in accordance with Sterlacchini et al. (2014) who reported that OMI-derived market value is suited for medium scale estimations (1:25000-1:50,000), with the main advantage of well distinguishing between areas of higher economic importance and economically marginal areas.

The area of interest of our work is composed of 33 municipalities; for each one on them the average market price for private houses is taken as reference (depending on the OMI zonation) and used to estimate exposure. The OMI database contains also information regarding the quotation of buildings used as offices (or as service sector in general), of commercial buildings (including shopping malls) and of industrial laboratories (including warehouses and sheds). For each of these categories the average market value is used again as reference. All the real estate market values extracted from the OMI database are reported in Table 1.

The exposure value of all the other buildings and roads categories is calculated on the basis of the construction/renovation cost for square meter. These values are tabulated by engineers or architects' associations in Valle d'Aosta or in other similar environments. Hotels are an example of this (Table 1). Their exposure range express the different construction costs of structures of different categories, with the highest values for luxury hotels. The construction cost is a good trade-off solution to be used when the market value cannot be used. This approach has been used by Peduto et al. (2018) by multiplying the construction cost for the footprint area, the number of the floors, and the height of each store of the building. Since our reference scale is different, we assumed exposure equal to the construction cost multiplied by 10 without adopting single buildings characteristic. It is recalled that the values of vulnerability of Table 1 are common for both the ADA-related and Model-related approaches; only landslide intensity is derived in two different ways.

Following the definition of Puissant et al. (2014), our methodology is aimed to derive a "macro-scale analysis" in which the final goal is "strategic regional planning" based on expert knowledge. For Puissant et al. (2014) the goals of such analysis are: 1) make an inventory of elements at risk, 2) rank their value for categories of structures and 3) select those elements at risk that could be impacted by a landslide. Only the potentially impacted elements are going to be considered at the macro-scale. We believe that our approach perfectly fits in the concept proposed Puissant et al. (2014) since, 1) we have a cadastral inventory, 2) we assign a market value or a construction cost to every building and 3) we use ADA as proxy for landslide impact.

3.5. Potential loss estimation

Once exposure and vulnerability (depending on the intensity level) are evaluated, the potential loss is calculated as product between vulnerability and exposure (Catani et al., 2005). The potential loss is referred to the direct impact of a landslide on a building or road and it is expressed in quantitative terms (Euros for square meters). If one or both vulnerability and exposure are null, the potential loss is obviously zero.

4. Results

The results of the previously illustrated methodology are presented here, through the selection of some case studies that highlight how vulnerability and potential loss are derived, using the two intensity approaches.

4.1. Deformation map

Despite the challenging environment, the MTInSAR processing of Sentinel-1 images gave good results in terms of spatial coverage of PS points and quality of measurements. A total of 364,451 PS points was obtained, with an average point density of 332 PS for square kilometer (Fig. 5).

The point distribution is strongly affected by land cover (i.e. presence of vegetation and perennial snow) and local morphology. The maximum density is registered along the Dora Baltea Valley (see Fig. 1 for the localization) where Aosta, the major city of VdA, is located and where the urbanization is higher. Along the tributary valleys the density will be again higher in correspondence of small cities and hamlets and where the mountain flanks orientation, slope and land cover allow a proper PS identification. On the other hand, PS density will be minimum, tending to zero, where the local morphological conditions create strong foreshortening, layover (i.e. along east-facing slopes, given the descending acquisition geometry) shadowing effects (i.e. along steep west-facing slopes) and where woods and perennial ice covers are present.

Within the PS velocity, the stability threshold criteria were based on the statistical analysis of the PS data population characterized by an approximately normal (Gaussian) distribution. The stability threshold was fixed at ± 5 mm/year, which is equal to the standard deviation value of the dataset, representing the dispersion of data around zero (Bianchini et al., 2013). Considering the stability threshold of 5 mm/yr, the 93 % of the PS points is considered "stable", meaning that the point is motionless or that the motion cannot be distinguished from the noise. Some moving areas, made by tens of PS points, are already visible at this scale; these areas are connected to the slow motion (usually below 10 mm/yr) of large deep-seated landslides that affect some portion of the area of interest (Solari et al., 2019).

4.2. ADA database

The ADA database was generated in an automated way, following the previously presented methodology. We obtained a total of 54 ADA composed by a minimum of 5 PS points with LOS velocities higher than 10 mm/yr (i.e. two times the standard deviation of the interferometric dataset). The largest part of the ADA registers average velocities between 10 and 20 mm/yr (76 % of the total); only few ADA exceed 30 mm/yr (Fig. 6). The ADA are well distributed in the area of interest, preferably along west-facing slopes at different altitudes. The distribution is affected by the satellite LOS in descending orbit with respect to slope aspect and angle; some east-facing flanks are simply impossible to measure because of geometrical effects. No moving areas are found along valley bottoms, meaning the absence of subsidence motions with high deformation rates.

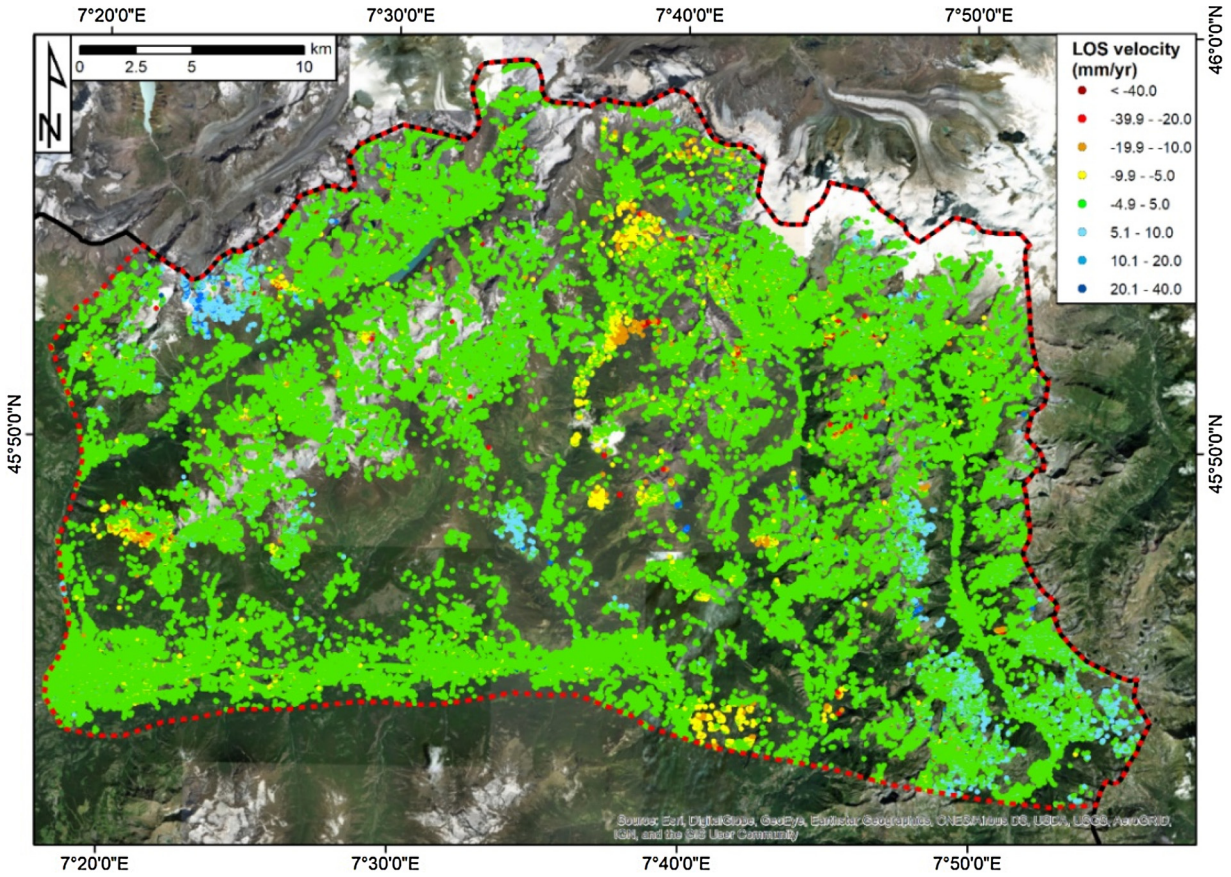

Fig. 5. Deformation map for the area of interest (red contour) obtained from Sentinel-1 radar images acquired in descending orbit. The background image is an ESRI World Imagery map (For interpretation of the references to colour in this figure legend, the reader is referred to the web version of this article.).

Considering the input conditions presented in Section 3.3, 15 ADA have been used to determine intensity using the ADA-related approach. Most of the ADA have been used as source areas for debris flow modelling, evaluating intensity on the basis of the Model-related approach. Nine ADA were not used for any intensity evaluation, as they do not fulfil the input conditions of our approach, and they were not exploited for vulnerability and potential loss evaluation.

4.3. Some examples of vulnerability and potential loss estimation

The first three examples came from the Valtournenche and Ayas Valleys, located in the eastern portion of the area of interest. Considering the direct overlapping between ADA and elements at risk, landslide intensity has been estimated using the ADA-related approach. The derived potential loss maps are shown in Fig. 7.

Inset 1 of Fig. 7 refers to the Cielo Alto hamlet in the southern portion of Breuil-Cervinia one of the main and most famous ski resorts in VdA. Three ADA are found in this area, affecting some elements at risk and fulfilling the input condition of the ADA-related approach. From a geomorphological point of view, the ADA are found along a west-facing slope between 2050 and 2150 m a.s.l. The area is characterized by the presence of a large DSGSD ("Cime Bianche" DSGSD) that affects the whole valley flank from an altitude of 2900 m a.s.l. to the valley bottom. The DSGSD occupies an area of 8 km^2. Its evolution is mainly related to deglaciation processes and subordinated fluvial activity; the presence of weak levels of pseudocarnioles and evaporites (Mont Fort Unit – Sartori, 1987), acting as basal shear plane, is the main controlling factor of the landslide (Martinotti et al., 2011). The motion of the Cime Bianche DSGSD is known, especially in its lower and marginal portion, as testified by the presence of tilted walls and damaged buildings (Martinotti et al., 2011). The ADA are found within the toe area of the Cime Bianche DSGSD, where Giordan et al. (2017) already reported the highest displacement rates by analyzing RADARSAT-1 interferometric data. See Fig. S1 for the localization of the ADA with respect to the DSGSD contour.

The ADA intensity is equal to 1, since all ADA average velocities are lower than 16 mm/yr. The velocity sign is negative and coherent with a motion along slope, away from the satellite LOS. The elements at risk in this area are mainly residential buildings, composed by 3–5 floors residences. A shopping mall and a restaurant are present as well. For landslide intensity equal to 1, vulnerability ranges between 0.15 and 0.3 for buildings and equal to 0.6 for roads (Fig. S4—inset 1). Considering a value of exposure for private houses equal to 2450 €/m^2, the potential loss is equal to 490 €/m^2 (Fig. 8—inset 1). The highest potential loss (532 €/m^2) is registered by a four-stars hotel; the lowest (21 €/m^2) by a tennis court.

Inset 2 of Fig. 8 presents the results obtained in Chaloz, one of the main villages of the Valtournenche municipality, 9 km south than Cielo Alto. The moving areas are detected along a west-facing slope in which several landslides are mapped (Fig. S2). In particular, a large DSGSD ("Valtournenche" DSGSD) involves the entire flank on which the Chaloz hamlet is located, from a height of 2900 m a.s.l. to 1500 m a.s.l. The activity of the Valtournenche DSGSD has been already testified by Giordan et al. (2017). These authors showed that the landslide can be subdivided into different sectors with different velocities, as testified by the ADA distribution obtained from Sentinel-1 data (Fig. S2). In addition to the DSGSD, 7 rotational landslides are mapped in the toe area of the deep-seated phenomenon (Fig. S2).

Four ADA are found within the Chaloz hamlet with average LOS velocities between 11 and 16 mm/year; intensity is then equal to 1 for all the ADA. Several buildings of the Chaloz hamlet are exposed to landslide risk; in particular, 390 structures are found within the contour

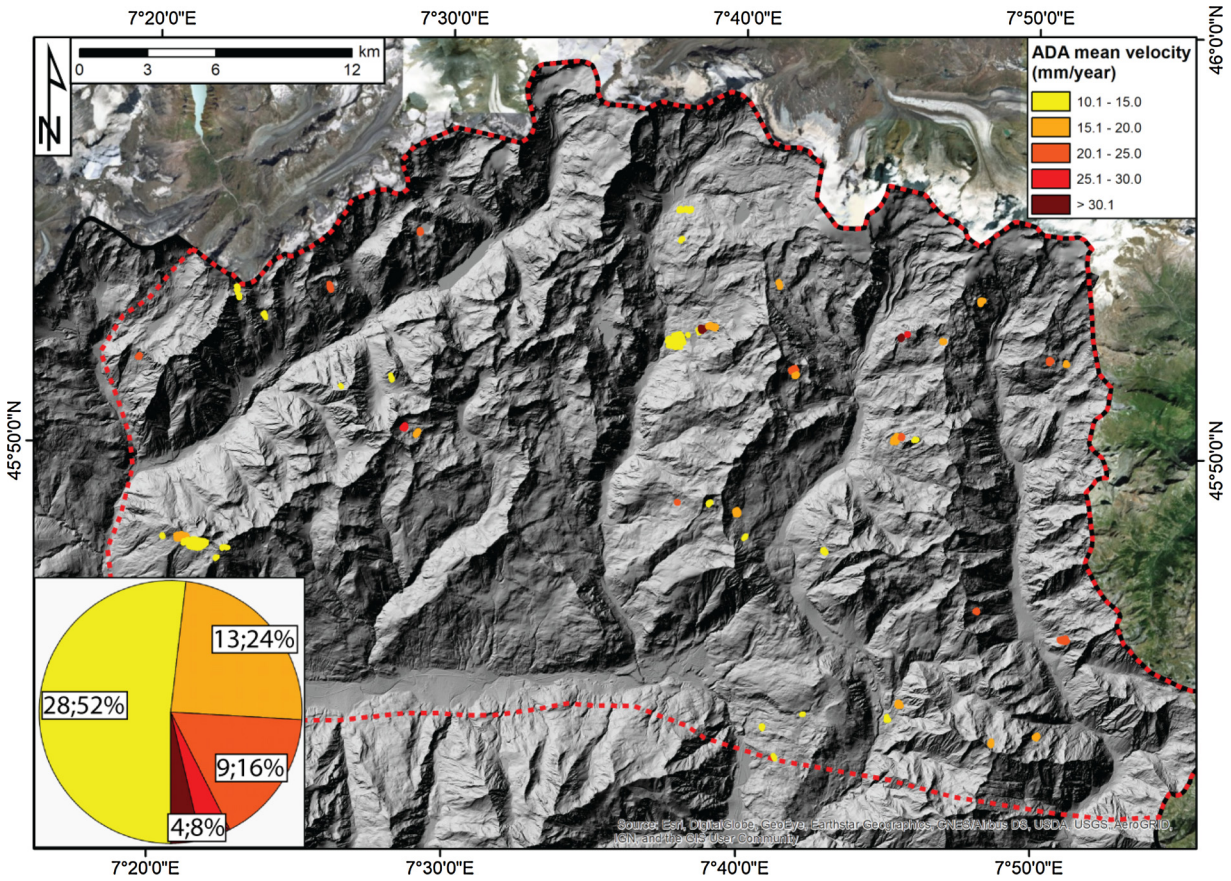

Fig. 6. ADA map for the area of interest. Each ADA is classified on the mean velocity value, obtained by averaging the velocities of all the PS points that form the moving area. The ADA map is overlaid on a 10 m DEM-derived hillshade. The background image is an ESRI World Imagery map.

of the ADA. Of these, 90 % are private houses; some shops, warehouses, four hotels, barns and a tennis court are present as well. Some local roads and a provincial road cut through the area of interest. Considering the type of edifice/road and the intensity level, vulnerability varies between 0.1 and 0.2 for buildings and between 0.4 and 0.6 for roads (local roads are more vulnerable than provincial roads, Fig. S4—inset 2). The potential loss ranges between 21 and 490 €/m^2; the highest value is reached by private houses (Fig. 7 — inset 2).

Inset 3 of Fig. 7 illustrates another example of ADA used for landslide intensity. The ADA is found in the Alésaz hamlet, part of the Challand Saint Anselme municipality in the southern portion of the Ayas Valley (Fig. 1). In this area, an ADA with intensity equal to 1 is found, affecting 100 elements at risk, mainly composed by private houses, but also including some barns and a school. A local road crosses the moving area. The village of Alèsaz rises on the lowermost portion of a complex landslide (1.8 km long and 600 m large) whose crown area is located 600 m above the village, at an altitude of 1770 m a.s.l. (Fig. S3). The activity of this landslide is demonstrated by the presence of two ADA, one affecting the village of Alèsaz and one the uppermost portion of the landslide, where elements at risk are not found (Fig. S3). Considering the landslide intensity (equal to 1) and the type of elements at risk, vulnerability ranges between 0.2 and 0.3 (Fig. S4—inset 3) whereas the potential loss varies between 16 and 1200 €/m^2. In the Valtournenche municipality the market value of private houses is lower than in the Challand Saint Anselme municipality; considering the same value of intensity and vulnerability, the potential loss will be lower in this second case, despite the same building typology. The highest value of potential loss is reached by the school located in the southern portion of the ADA affecting the village of Alèsaz (Fig. 8 —inset 3).

Figs. 8 and 9 present two examples of potential loss maps derived using the Model-related intensity approach. Both case studies are taken from the Montjovet municipality in the Lower VdA, on the left flank of the Dora Baltea Valley. The ADA of interest are located along the same slope, 1.5 km apart from each other. The input parameters of the model can be found in Section 3.3 and have been used for both case studies, assuming the same geological context in a similar morphological environment.

The first example shows an ADA located few hundred meters above the village of Ciseran. The whole valley flank is affected by a large DSGSD ("Emarese" DSGSD) whose crown is located at 1800 m.a.s.l., 1000 m above the moving area (Fig. S5). The slow motion of this landslide has been already measured using ERS 1/2 interferometric data (Broccolato and Paganone, 2012). No other landslides are found in this area (Fig. S5). The moving area does not directly intersect any element at risk, but, considering the presence of debris material, the GPP model is applicable to determine landslide intensity. Two source areas (S1 and S2 in Fig. 8) are extracted from the ADA and selected to run the model. The ADA is found on the upper portion of the watershed; therefore, the flows directions are divergent. From S1 the debris follows the slope morphology along the WNW direction, depositing the maximum height of material (2.5 m) at an altitude of 650 m a.s.l. The second debris flow, originated in S2, follows a WSW direction, filling a small depression located at an altitude of 770 m a.s.l. and depositing the remaining available material between 625 and 660 m a.s.l. (Fig. 8). The material deposited by the flow originated from S1 does not interact with any element at risk, whereas the flow having S2 as source area hits a house located 150 m below. The height of the material in correspondence of the building is below 1.25 m (intensity 1). The vulnerability value is 0.2 and, estimating an exposure of 1300 €/m^2, the potential damage is equal to 260 €/m^2.

The second example of Model-related intensity is presented in Fig. 9. Tron hamlet is located within the contours of one DSSGD and

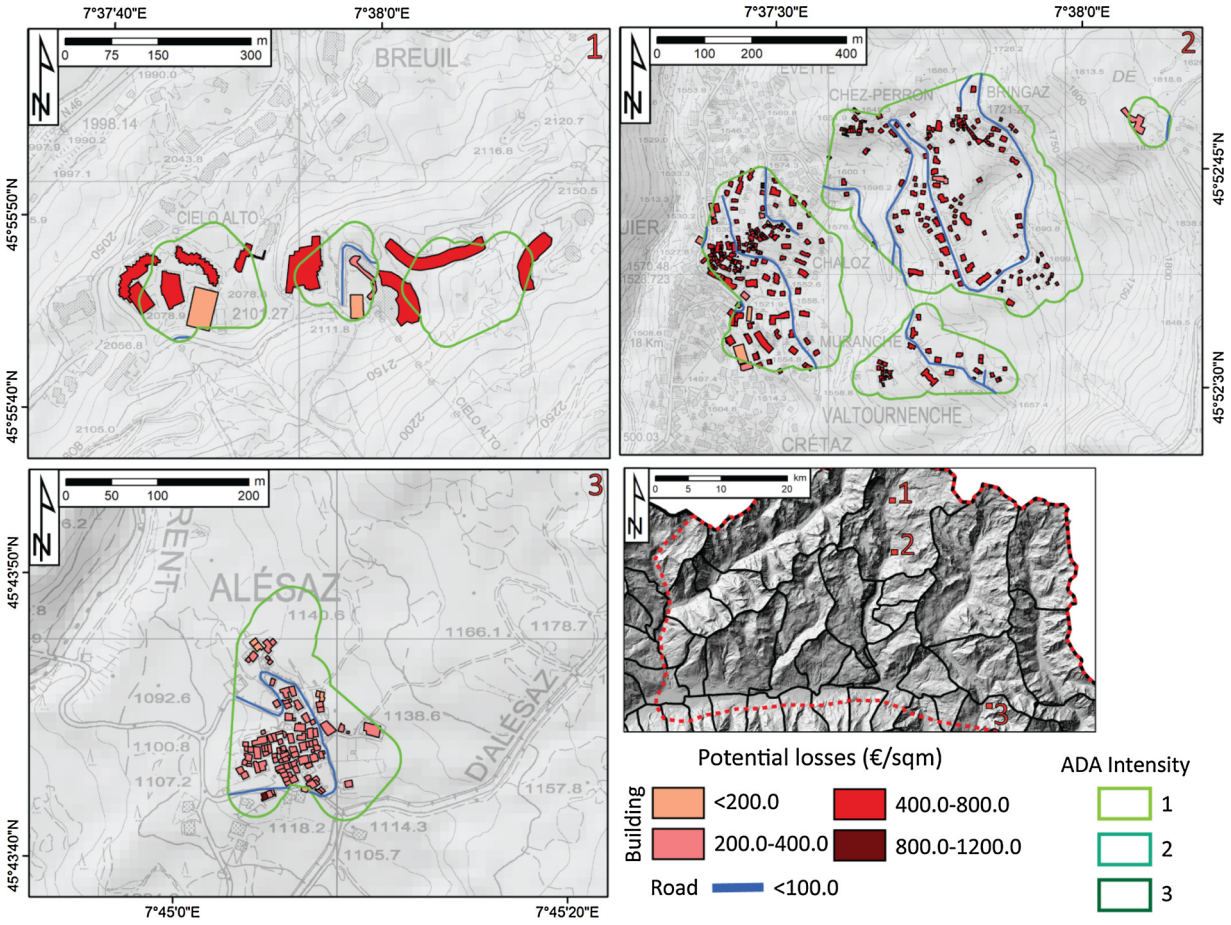

Fig. 7. Potential loss maps derived using the ADA-related intensity approach. The examples 1 and 2 are taken from the Valtournenche Valley, municipality of Valtournenche; the example 3 is taken from the municipality if Challand-Saint Anselme, at the Ayas Valley mouth. The maps are overlaid on a 1:10,000 cadastral map of the VdA region.

two complex landslides connected to the geometry and evolution of the Emarese DSGSD (Fig. S6). The ADA is located in the upper portion of these landslides, where debris deposits are found. The motion of this sector has been also reported by Broccolato and Paganone (2012) for ERS 1/2 data. The GPP model is exploited to simulate the run-out of debris flows from two different source areas (S1 and S2 in Fig. 9). The thickness of the material for S1 is between 2 and 2.4 m, whereas for S2 the input material thickness is lower, varying between 0.6 and 1 m. The flows originated from the two source areas converge and create a fan-like deposit with variable thickness between 0.2 and 1.6 m (intensity 1). The flow does not involve any building but two local roads. Considering an exposure of 50 €/m^2 and a vulnerability of 0.6, the resulting potential damage is 30 €/m^2.

5. Discussions

In this work, we exploited the demonstrated potential of satellite interferometric data for geohazard mapping (focusing on landslides) in a new way, by developing a procedure aimed to estimate vulnerability and potential loss of structures and infrastructures at regional scale. Here, interferometric results, intended as ADA or in general moving "hot-spots", are the key input for landslide intensity and vulnerability estimation which, combined with the exposure of the elements at risk, allow to calculate the potential loss of a structure. The concept of "PS hot-spot" is not new in literature (see for example Bianchini et al., 2012), but the use of moving areas for quantitative or qualitative estimation of landslide impact on built-up areas is uncommon. Some examples of vulnerability estimation from interferometric data are present in literature. Solari et al., 2018, used a qualitative classification of elements at risk depending on MTInSAR ground velocity maps and on the strategic use of buildings in different civil protection phases. Peduto et al. (2017), took advantage of PS data for fragility and vulnerability curves generation. Usually, interferometric products are a support for landslide activity evaluation (i.e. Rosi et al., 2018), for landslide intensity measures (i.e. Cigna et al., 2013) or landslide mapping (i.e. Strozzi et al., 2005; Barra et al., 2016; Cignetti et al., 2016; Dini et al., 2019). Recently, Intrieri et al. (2018) and Raspini et al. (2018) showed innovative usages for PS data as near-real-time tools for landslide forecasting. It must be recalled that interferometric data are rarely used for quantitative risk estimation (Lu et al., 2014). Thus, our methodology represents one of the few attempts of this kind. This work aims to bridge the gap that exists between retrieving the interferometric information on landslide phenomena, which is a nowadays a well-established field, and feeding these data into hazard and risk assessments procedure.

The methodology relies on MTInSAR data in three different ways: 1) as proxy for ground movement hot-spots (i.e. the ADA), 2) as landslide intensity tool ("ADA-related" approach) and 3) as an effort to detect potential source areas of debris flow ("Model-related" approach). The latter represents an original approach for interferometric data exploitation and has been specifically designed to be implemented in mountainous regions at basin scale or smaller. In the Model-related approach the interferometric data are both a proxy for moving debris deposits and an input for the GPP model, acting as the main factor for the source areas definition. In this way, it is possible to improve the information extracted from each ADA by assuming that a debris

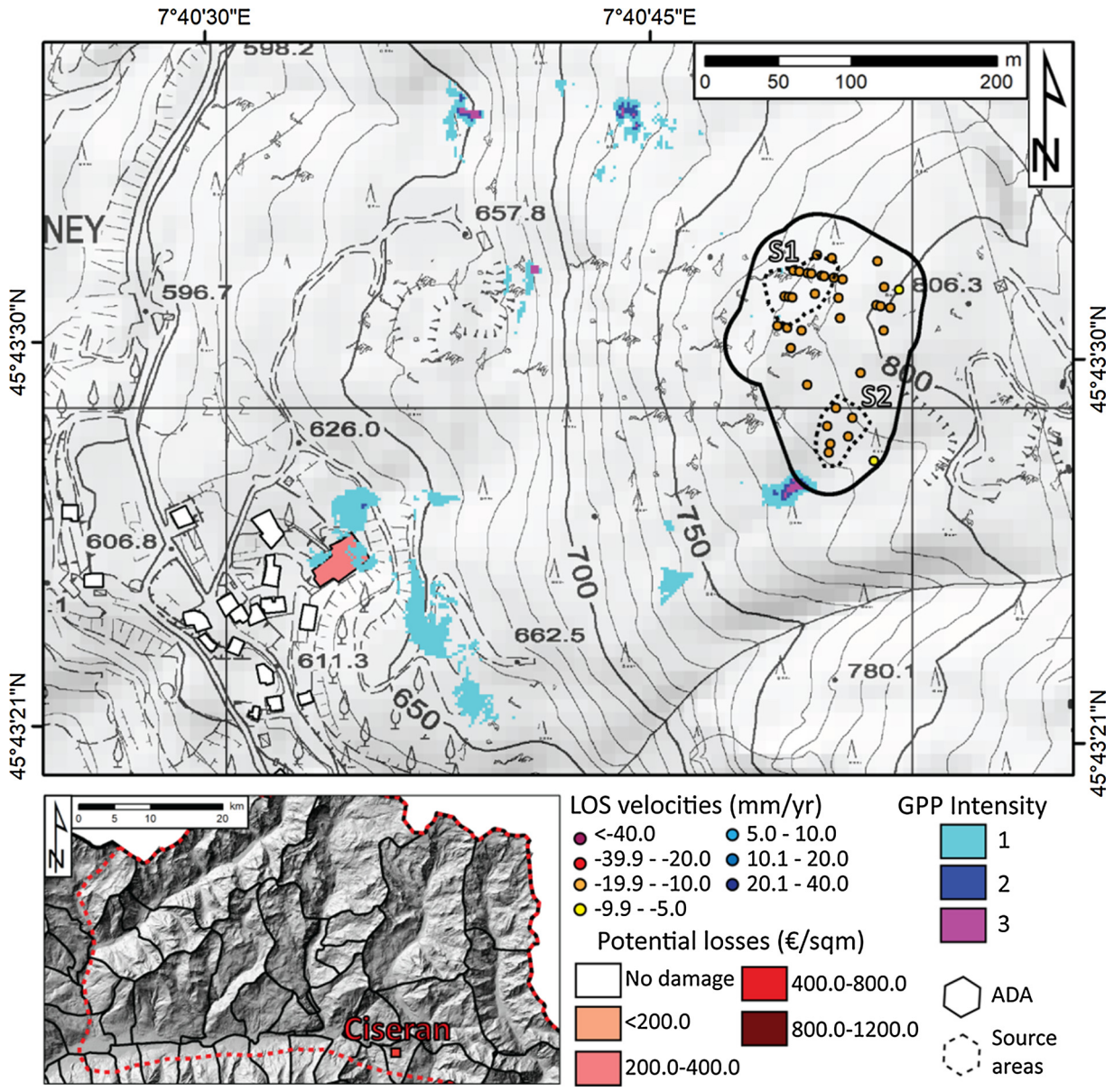

Fig. 8. Landslide potential loss derived using the Model-related intensity approach for the village of Ciseran in the Montjovet municipality. S1 and S2 are referred to the two source areas chosen to run the GPP model. The background image is a 1:10,000 cadastral map of the VdA region.

deposit, already in motion (as testified by the PS data), could evolve into a debris flow if external triggering factors are present (i.e. an intense rainfall period). The distinction between superficial motions and DSGSD long-term movement is one of the potential mismatches of the methodology. We solved this by considering a velocity threshold higher than the maximum average annual velocity value of DSGSD along the Alpine Arc (1 cm/yr - Crosta et al., 2013). Secondly, DSGSD classically show a peculiar flank-scale pattern in which outlier velocities can be easily detected by the ADA. We consider these areas as representative for superficial motions and we select, depending on the presence of geoindicators, the targets for the GPP model. The focus of our work is in a direct way those landslides showing the highest deformation rates in VdA (complex or rotational) or indirectly the source areas of potential debris flows. We point out that the approach is not aimed to obtain landslide contours, but it can be integrated into existing landslide catalogues (such as IFFI) for estimating the state of activity of these phenomena.

Our methodology is designed for regional scale studies with few ancillary data available. It relies on small scale interferometric products, based on strict thresholding rules for better limiting atmospheric artifacts and noise in general, and on a basin/flank-scale runout model. The latter requiring only, in its simplest configuration, a DEM of the slope and a potential source area. Thus, it has not been designed for single landslide characterization. We believe that, although more detailed geomorphological investigations would be required (including an in situ campaign), our approach can offer useful results for future detailed scale analysis. In medical terms, we can define the methodology as a preliminary screening defining where is the pain without fully addressing the symptoms.

The output of the methodology are simple color-scale maps showing the intensity of the potential landslide (as ADA velocity or as height of material deposited by a debris flow) and a value of potential loss (in €/m^2), expression of vulnerability (depending on landslide intensity) and exposure (defined as real estate market values) of the elements at risk. The potential loss is not directly related to the real repair cost which is impossible to quantitatively estimate at regional scale, without having access to more detailed building characteristics and renovation costs. The potential end-users, such as Civil Protection entities,

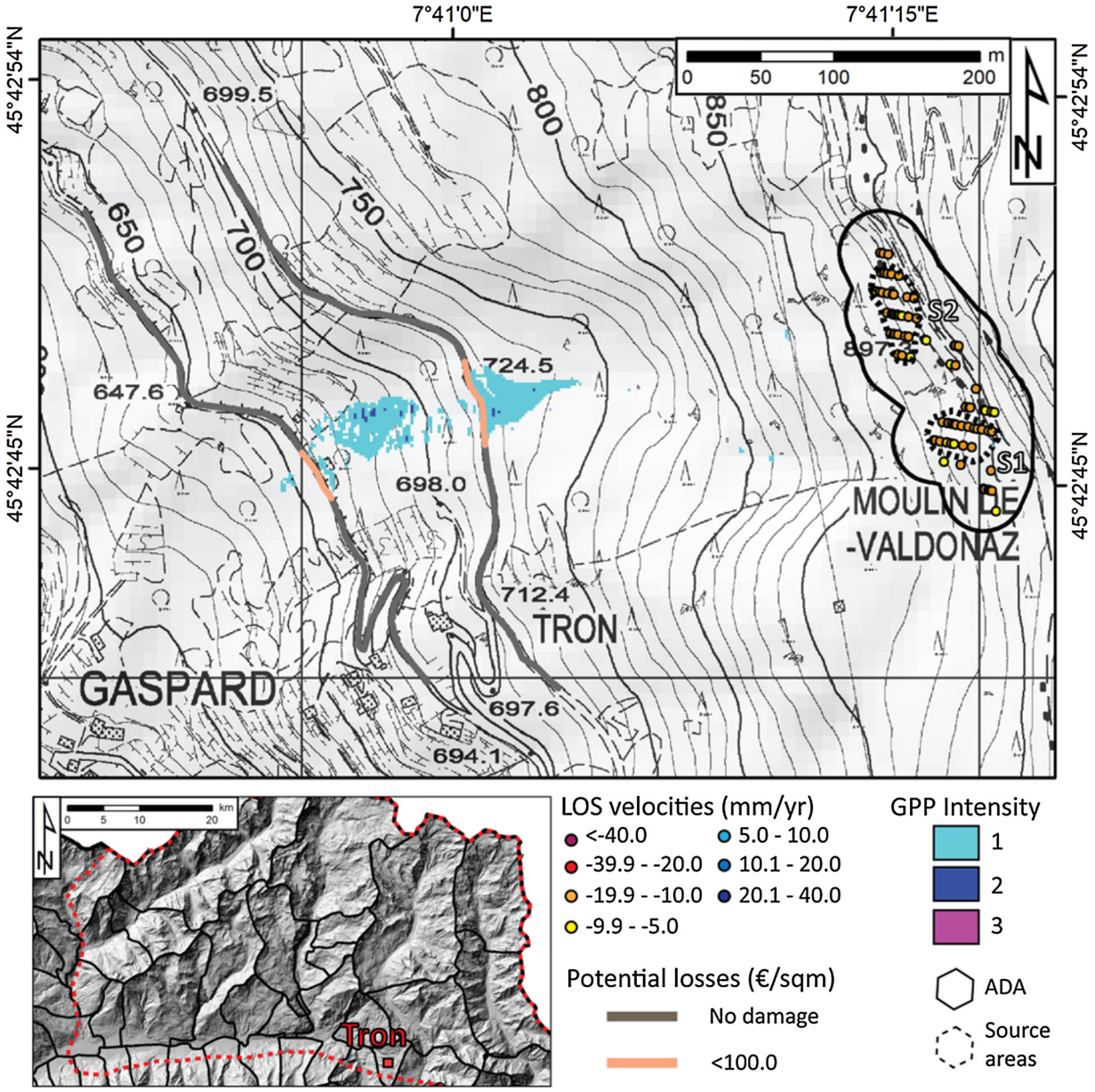

Fig. 9. Landslide potential loss derived using the Model-related intensity approach for the hamlet of Tron in the Montjovet municipality. S1 and S2 are referred to the two source areas chosen to run the GPP model. The background image is a 1:10,000 cadastral map of the VdA region.

emergency responders, as well as risk management actors and insures, can easily know which are the areas that are moving faster, and which is their potential impact on built-up areas.

The working scale is at the same time an advantage and a limitation. On one side, it is possible to promptly detect those areas showing the highest displacement rates and verify if they affect or could affect one or more elements at risk. On the other side, some assumptions must be made, especially when configuring the GPP model and when selecting the source areas. The economic value of each element at risk cannot be assessed precisely because detailed information about the state of conservation of buildings and roads cannot be gathered in short time over entire basins. The population has not been considered in this work due to the difficulties in estimating day/night occupancy of each edifice. Nevertheless, as further future perspective of this work, the quantification of the human value at risk in the area could be estimated. A possible solution should define a rough people's vulnerability by looking at public buildings (hotels, schools etc.) and private houses, which are inhabited all-year round or rented for holiday. This analysis could be done only for selected test sites and focused on a worst-case scenario (e.g. day time for schools, i.e. period with maximum occupancy) to provide the maximum potential degree of loss.

A relevant approximation concerns the velocity threshold used to derive the ADA; although it depends on the quality of the interferometric dataset (standard deviation) it assures to take into account and select motions with high deformation rates only, not considering extremely slow deformation that could create damage to buildings and roads over very long periods.

Considering its limitations, the methodology is able to provide useful outputs for risk management at regional scale in a short time. In fact, the selection of moving areas and the calculation of exposure, vulnerability and potential loss requires 2 or 3 weeks of work of an expert in the field of satellite interferometric data interpretation. The same amount of time is required to analyze the SAR images and derive the deformation map. Some phases of the methodology are quite fast, as the generation of moving areas by applying the ADA-finder package (less than a minute). This time requirements allow for the setting up of

a monitoring plan based on 4 or 5 updates of the deformation map every year, re-evaluating each time landslide intensity and the potential damage that could be experienced by buildings and roads, analyzing at the same time the temporal evolution of the phenomena.

The use of the ADA database is practical and useful for quickly and automatically highlighting the fastest moving areas at wide scale and it depends on complying with some input conditions in order to select the suitable approach for the landslide intensity evaluation. Nevertheless, as another limitation of the methodology, it is worth to note that the exploitation of ADA must be carefully performed, since the ADA interpretation does not specifically refer to the type of landslide. Conversely, the moving areas automatically detected by ADA could represent a well-defined failure mechanism within a landslide or it could be just a part of a wider ground motion on a slope; as a result, beyond the limiting conditions of ADA, a robust manual interpretation and validation of such areas of movements should be always carried out to better define and understand them within the dynamics and morphological setting of the selected area of interest.

Our approach is made for a wider exploitation of interferometric products, not only as mapping tools but also as instruments for preliminary risk quantification. The use of both ascending and descending acquisition modes is highly recommended, especially in mountainous areas where shadowing and foreshortening effects prevent the mountainsides to be efficiently seen by the satellite. Unluckily, data acquired by only one orbit were here available, and the elaboration of both acquisition geometries is expected for future work. The acquisition of MTInSAR product over wide areas can be demanding from the point of view of the computational power and rather expensive if in-house processing tools or if open-source codes are not available. In this context, the future launch of the European Ground Motion Service will grant a wider free access to interferometric data (EU-GMS Task Force, 2017). The availability of Sentinel-1 data at regional and national scale will require new efforts for a correct interpretation and dissemination of the results, including a proper definition of downstream services. We believe that our methodology represents an attempt to meet the requirements of this new way of distributing and exploiting satellite interferometric results.

6. Conclusions

This paper presents a methodology for landslide intensity estimation based on satellite interferometric products. The deformation map derived from a MTInSAR analysis of Sentinel-1 radar images is the starting point of the procedure. The first product is the hot-spots of deformation "ADA" and the final goal is estimating potential loss experienced by one or more elements at risk (building and roads) under a given level of landslide intensity (derived in a twofold manner). The final product is a preliminary risk map which includes the definition of all the critical facilities ranked by potential damage or risk. The methodology has been tested in Eastern Valle d'Aosta (north-western Italy) along four lateral valleys of the Dora Baltea Valley, in a territory characterized by steep slopes and widespread landslides and debris deposits.

Fifty-four ADA have been derived from the deformation map of these, 15 have been used for the ADA-related intensity analysis and 30 for the Model-related analysis. The two approach differ in the way in which the ADA are used for landslide intensity evaluation: as direct estimation of landslide magnitude (and thus intensity) and as an indicator for the presence of unstable debris deposits that could be the source areas of future debris flows, whose runout is foreseen by means of the GPP model. Five case studies have been proposed to illustrate how the two approaches converge to obtain potential loss maps.

In summary, the methodology is able to highlight the fastest motions (detectable from space) at regional scale and then, by estimating the value of the elements at risk and landslide intensity, derive color-scale maps of potential loss expressed in quantitative terms. Considering the current availability of 6-days C-band Sentinel-1 image with an "open-source" delivery strategy and the future plan of a European deformation map, this sort of methodology represents an example of supporting tool for interferometric data interpretation and dissemination.

Declaration of Competing Interest

The authors declare that they have no known competing financial interests or personal relationships that could have appeared to influence the work reported in this paper.

Acknowledgements

This work has been funded by the European Commission, Directorate-General Humanitarian Aid and Civil Protection (ECHO), through the project U-GEOHAZ – Geohazard Impact Assessment for Urban Areas. Grant Agreement No. 783169.

Appendix A. Supplementary data

Supplementary material related to this article can be found, in the online version, at doi:https://doi.org/10.1016/j.jag.2019.102028.

References

Barra, A., Monserrat, O., Mazzanti, P., Esposito, C., Crosetto, M., Scarascia Mugnozza, G., 2016. First insights on the potential of Sentinel-1 for landslides detection. Geomat. Nat. Hazards Risk 7 (6), 1874–1883. https://doi.org/10.1080/19475705.2016.1171258.

Barra, A., Solari, L., Béjar-Pizarro, M., Monserrat, O., Bianchini, S., Herrera, G., Crosetto, M., Sarro, R., González-Alonso, E., Mateos, R.M., Ligüerzana, S., López, C., Moretti, S., 2017. A methodology to detect and update Active Deformation Areas based on Sentinel-1 SAR images. Remote Sens. 9 (10), 1002. https://doi.org/10.3390/rs9101002.

Bell, R., Glade, T., 2004. Quantitative risk analysis for landslides–Examples from Bíldudalur, NW-Iceland. Nat. Hazards Earth Syst. Sci. 4 (1), 117–131. https://doi.org/10.5194/nhess-4-117-2004.

Bianchini, S., Cigna, F., Righini, G., Proietti, C., Casagli, N., 2012. Landslide hotspot mapping by means of persistent scatterer interferometry. Environ. Earth Sci. 67 (4), 1155–1172. https://doi.org/10.1007/s12665-012-1559-5.

Bianchini, S., Herrera, G., Mateos, R.M., Notti, D., Garcia, I., Mora, O., Moretti, S., 2013. Landslide activity maps generation by means of persistent scatterer interferometry. Remote Sens. 5 (12), 6198–6222. https://doi.org/10.3390/rs5126198.

Bianchini, S., Raspini, F., Ciampalini, A., Lagomarsino, D., Bianchi, M., Bellotti, F., Casagli, N., 2017a. Mapping landslide phenomena in landlocked developing countries by means of satellite remote sensing data: the case of dilijan (Armenia) area. Geomatics Natural Hazard and Risk 8 (2), 225–241. https://doi.org/10.1080/19475705.2016.1189459.

Bianchini, S., Solari, L., Casagli, N., 2017b. A GIS-based procedure for landslide intensity evaluation and specific risk analysis supported by persistent scatterers interferometry (PSI). Remote Sens. 9 (11), 1093. https://doi.org/10.3390/rs9111093.

Biescas, E., Crosetto, M., Agudo, M., Monserrat, O., Crippa, B., 2007. Two radar interferometric approaches to monitor slow and fast land deformation. J. Surv. Eng. 133 (2), 66–71. https://doi.org/10.1061/(asce)0733-9453(2007)133:2(66).

Bistacchi, A., Dal Piaz, G.V., Massironi, M., Zattin, M., Balestrieri, M.L., 2001. The Aosta–Ranzola extensional fault system and Oligocene Present evolution of the Austroalpine–Penninic wedge in the north-western Alps. International Journal of Earth Sciences (Geologisches Rundschau) 90 (3), 654–667. https://doi.org/10.1007/s005310000178.

Broccolato, Paganone, 2012. Grandi frane permanenti complesse - schede monografiche di frane in Valle d'Aosta analizzate con tecnica PS. Attività B2/C2 Rischi idrogeologici e da fenomeni gravitativi - Progetto Strategico Interreg IVa Risknat. Available online. http://www.risknet-alcotra.org/rna/allegati/risknat-b2-c2-schede-frane-vda_1023.pdf.

Carraro, F., Giardino, M., 2004. Quaternary glaciations in the Western Italian Alps – a review. In: Ehlers, J., Gibbard, P.L. (Eds.), Quaternary Glaciations – Extent and Chronology. Part 1. Developments in Quaternary Science. https://doi.org/10.1016/s1571-0866(04)80071-x. 2, 201–208.

Catani, F., Casagli, N., Ermini, L., Righini, G., Menduni, G., 2005. Landslide hazard and risk mapping at catchment scale in the Arno River basin. Landslides 2 (4), 329–342. https://doi.org/10.1007/s10346-005-0021-0.

Catani, F., Segoni, S., Falorni, G., 2010. An empirical geomorphology-based approach to the spatial prediction of soil thickness at catchment scale. Water Resour. Res. 46 (5). https://doi.org/10.1029/2008wr007450.

Catani, F., Tofani, V., Lagomarsino, D., 2016. Spatial patterns of landslide dimension: a tool for magnitude mapping. Geomorphology 273, 361–373. https://doi.org/10.1016/j.geomorph.2016.08.032.

Cigna, F., Bianchini, S., Casagli, N., 2013. How to assess landslide activity and intensity

with Persistent Scatterer Interferometry (PSI): the PSI-based matrix approach. Landslides 10 (3), 267–283. https://doi.org/10.1007/s10346-012-0335-7.
Cignetti, M., Manconi, A., Manunta, M., Giordan, D., De Luca, C., Allasia, P., Ardizzone, F., 2016. Taking advantage of the esa G-pod service to study ground deformation processes in high mountain areas: A valle d'aosta case study, northern Italy. Remote Sens. 8 (10), 852. https://doi.org/10.3390/rs8100852.
Conrad, O., Bechtel, B., Bock, M., Dietrich, H., Fischer, E., Gerlitz, L., Wehberg, J., Wichmann, V., Böhner, J., 2015. System for automated geoscientific analyses (SAGA) v. 2.1. 4. Geoscientific Model Development 8 (7), 1991–2007. https://doi.org/10.5194/gmd-8-1991-2015.
Corominas, J., van Westen, C., Frattini, P., Cascini, L., Malet, J.P., Fotopoulou, S., Catani, F., Van Den Eeckhaut, M., Mavrouli, O., Agliardi, F., Pitilakis, K., Winter, M.G., Pastor, M., Ferlisi, S., Tofani, V., Hervás, J., Smith, J.T., 2014. Recommendations for the quantitative analysis of landslide risk. Bull. Eng. Geol. Environ. 73 (2), 209–263. https://doi.org/10.1007/s10064-013-0538-8.
Costantini, M., Farina, A., Zirilli, F., 1999. A fast phase unwrapping algorithm for SAR interferometry. IEEE Trans. Geosci. Remote. Sens. 37 (1), 452–460. https://doi.org/10.1109/36.739085.
Crosetto, M., Monserrat, O., Cuevas, M., Crippa, B., 2011. Spaceborne differential SAR interferometry: data analysis tools for deformation measurement. Remote Sens. 3 (2), 305–318. https://doi.org/10.3390/rs3020305.
Crosetto, M., Monserrat, O., Cuevas-González, M., Devanthéry, N., Crippa, B., 2016. Persistent scatterer interferometry: a review. ISPRS J. Photogramm. Remote. Sens. 115, 78–89. https://doi.org/10.1016/j.isprsjprs.2015.10.011.
Crosta, G.B., Frattini, P., Agliardi, F., 2013. Deep seated gravitational slope deformations in the European Alps. Tectonophysics 605, 13–33.
Cruden, D.M., Varnes, D.J., 1996. Landslides: investigation and mitigation. Chapter 3. Landslide Types and Processes. Transportation research board special report 247.
Dai, F.C., Lee, C.F., Ngai, Y.Y., 2002. Landslide risk assessment and management: an overview. Eng. Geol. 64 (1), 65–87.
Del Ventisette, C., Righini, G., Moretti, S., Casagli, N., 2014. Multitemporal landslides inventory map updating using spaceborne SAR analysis. Int. J. Appl. Earth Obs. Geoinf. 30, 238–246. https://doi.org/10.1016/j.jag.2014.02.008.
Devanthéry, N., Crosetto, M., Monserrat, O., Cuevas-González, M., Crippa, B., 2014. An approach to persistent scatterer interferometry. Remote Sens. 6 (7), 6662–6679. https://doi.org/10.3390/rs6076662.
Dini, B., Manconi, A., Loew, S., 2019. Investigation of slope instabilities in NW Bhutan as derived from systematic DInSAR analyses. Eng. Geol. 259, 105–111.
EU-GMS Task Force, 2017. European Ground Motion Service (EU-GMS). A proposed Copernicus service element.
Fell, R., Corominas, J., Bonnard, C., Cascini, L., Leroi, E., Savage, W.Z., 2008. Guidelines for landslide susceptibility, hazard and risk zoning for land-use planning. Eng. Geol. 102 (3-4), 99–111. https://doi.org/10.1016/j.enggeo.2008.03.009.
Gamma, P., 2000. dfwalk-Ein Murgang-Simulationsprogramm zur Gefahrenzonierung. Geographisches Institut der Universität Bern.
Giordan, D., Cignetti, M., Bertolo, D., 2017. The Use of Morpho-Structural Domains for the Characterization of Deep-Seated Gravitational Slope Deformations in Valle d'Aosta. In Workshop on World Landslide Forum. May. Springer, Cham, pp. 59–68. https://doi.org/10.1007/978-3-319-53483-1_9.
Glade, T., Anderson, M.G., Crozier, M.J., 2006. Landslide Hazard and Risk. John Wiley & Sons.
Guzzetti, F., Galli, M., Reichenbach, P., Ardizzone, F., Cardinali, M.J.N.H., 2006. Landslide hazard assessment in the Collazzone area, Umbria, Central Italy. Nat. Hazards Earth Syst. Sci. 6 (1), 115–131. https://doi.org/10.5194/nhess-6-115-2006.
Hanssen, R., 2001. Radar Interferometry. Kluwer Academic Publishers, Dordrecht.
Herrera, G., Gutiérrez, F., García-Davalillo, J.C., Guerrero, J., Notti, D., Galve, J.P., Fernández-Merodo, J.A., Cooksley, G., 2013. Multi-sensor advanced DInSAR monitoring of very slow landslides: the Tena Valley case study (Central Spanish Pyrenees). Remote Sens. Environ. 128, 31–43. https://doi.org/10.1016/j.rse.2012.09.020.
Hölbling, D., Füreder, P., Antolini, F., Cigna, F., Casagli, N., Lang, S., 2012. A semi-automated object-based approach for landslide detection validated by persistent scatterer interferometry measures and landslide inventories. Remote Sens. 4 (5), 1310–1336. https://doi.org/10.3390/rs4051310.
Horowitz, E., Sahni, S., 1976. Fundamentals of Data Structures. Pitman books Ltd, London.
Hungr, O., 1997. Some methods of landslide hazard intensity mapping. In: Cruden, D., Fell, R. (Eds.), Landslide Risk Assessment. A.A. Balkema, Rotterdam, pp. 215–226.
Imaizumi, F., Nishiguchi, T., Matsuoka, N., Trappmann, D., Stoffel, M., 2018. Interpretation of recent alpine landscape system evolution using geomorphic mapping and L-band InSAR analyses. Geomorphology 310, 125–137. https://doi.org/10.1016/j.geomorph.2018.03.013.
Intrieri, E., Raspini, F., Fumagalli, A., Lu, P., Del Conte, S., Farina, P., Allevi, J., Ferretti, A., Casagli, N., 2018. The Maoxian landslide as seen from space: detecting precursors of failure with Sentinel-1 data. Landslides 15 (1), 123–133. https://doi.org/10.1007/s10346-017-0915-7.
Kaynia, A.M., Papathoma-Köhle, M., Neuhäuser, B., Ratzinger, K., Wenzel, H., Medina-Cetina, Z., 2008. Probabilistic assessment of vulnerability to landslide: application to the village of Lichtenstein, Baden-Württemberg, Germany. Eng. Geol. 101 (1-2), 33–48. https://doi.org/10.1016/j.enggeo.2008.03.008.
Ko, C.K., Flentje, P., Chowdhury, R., 2004. Landslides qualitative hazard and risk assessment method and its reliability. Bull. Eng. Geol. Environ. 63 (2), 149–165. https://doi.org/10.1007/s10064-004-0231-z.
Kumar, V., Venkataraman, G., 2011. SAR interferometric coherence analysis for snow cover mapping in the western Himalayan region. Int. J. Digit. Earth 4 (1), 78–90. https://doi.org/10.1080/17538940903521591.
Lari, S., Frattini, P., Crosta, G.B., 2012. Local scale multiple quantitative risk assessment and uncertainty evaluation in a densely urbanised area (Brescia, Italy). Nat. Hazards Earth Syst. Sci. Discuss. 12, 3387–3406.
Lateltin, O., Haemmig, C., Raetzo, H., Bonnard, C., 2005. Landslide risk management in Switzerland. Landslides 2 (4), 313–320. https://doi.org/10.1007/s10346-005-0018-8.
Liu, P., Li, Z., Hoey, T., Kincal, C., Zhang, J., Zeng, Q., Muller, J.P., 2013. Using advanced InSAR time series techniques to monitor landslide movements in Badong of the Three Gorges region, China. Int. J. Appl. Earth Obs. Geoinf. 21, 253–264. https://doi.org/10.1016/j.jag.2011.10.010.
Lu, P., Bai, S., Tofani, V., Casagli, N., 2019. Landslides detection through optimized hot spot analysis on persistent scatterers and distributed scatterers. ISPRS J. Photogramm. Remote. Sens. 156, 147–159.
Lu, P., Catani, F., Tofani, V., Casagli, N., 2014. Quantitative hazard and risk assessment for slow-moving landslides from Persistent Scatterer Interferometry. Landslides 11 (4), 685–696. https://doi.org/10.1007/s10346-013-0432-2.
Martinotti, G., Giordan, D., Giardino, M., Ratto, S., 2011. Controlling factors for deep-seated gravitational slope deformation (DSGSD) in the Aosta Valley (NW Alps, Italy). Geol. Soc. London Spec. Publ. 351 (1), 113–131. https://doi.org/10.1144/sp351.6.
Mavrouli, O., Corominas, J., 2010. Vulnerability of simple reinforced concrete buildings to damage by rockfalls. Landslides 7 (2), 169–180. https://doi.org/10.1007/s10346-010-0200-5.
Navarro, J.A., Cuevas, M., Barra, A., Crosetto, M., 2018. Detection of active deformation areas based on sentinel-1 imagery: an efficient, fast and flexible implementation. In: Proceedings of 18th International Scientific and Technical Conference. Crete, Greece, September 24-27.
Palomba, M., Giardino, M., Ratto, S., Pogliotti, P., 2015. Analysis of factors controlling landslide susceptibility in the aosta Valley (NW Italy): relationship to climatic and environmental changes. EngineEring Geology for Society and Territory Volume 1. Springer, Cham, pp. 435–438. https://doi.org/10.1007/978-3-319-09300-0_83.
Papathoma-Köhle, M., Totschnig, R., Keiler, M., Glade, T., 2012. A new vulnerability function for debris flow-the importance of physical vulnerability assessment in alpine areas. In: Koboltschng, G., Hübl, J., Braun, J. (Eds.), Internationales Symposion Interpraevent, Genoble, April 23–26, 2012. Internationale Forschungsgesellschaft Interpraevent (2012), Klagenfurt, pp. 1033–1043.
OMI database, 2018. Agency of Revenues. (accessed 20 May 2019). https://wwwt.agenziaentrate.gov.it/geopoiomi/index.php.
Pastonchi, L., Barra, A., Monserrat, O., Luzi, G., Solari, L., Tofani, V., 2018. Satellite data to improve the knowledge of geohazards in world heritage sites. Remote Sens. 10 (7), 992. https://doi.org/10.3390/rs10070992.
Peduto, D., Ferlisi, S., Nicodemo, G., Reale, D., Pisciotta, G., Gullà, G., 2017. Empirical fragility and vulnerability curves for buildings exposed to slow-moving landslides at medium and large scales. Landslides 14 (6), 1993–2007. https://doi.org/10.1007/s10346-017-0826-7.
Peduto, D., Nicodemo, G., Caraffa, M., Gullà, G., 2018. Quantitative analysis of consequences to masonry buildings interacting with slow-moving landslide mechanisms: a case study. Landslides 15 (10), 2017–2030. https://doi.org/10.1007/s10346-018-1014-0.
Pellicani, R., Van Westen, C.J., Spilotro, G., 2014. Assessing landslide exposure in areas with limited landslide information. Landslides 11, 463–480. https://doi.org/10.1007/s10346-013-0386-4.
Petley, D.N., Dunning, S.A., Rosser, K., Rosser, N.J., 2005. The analysis of global landslide risk through the creation of a database of worldwide landslide fatalities. In: Hunger, O., Fell, R., Couture, R., Ebberhardt, E. (Eds.), Landslide Risk Management. Balkema, Amsterdam, June 30, 2005. Taylor & Francis Group, London, UK, pp. 367–373 2005.
Polino, R., Dal Piaz, G.V., Gosso, G., 1990. Tectonic erosion at the Adria margin and accretionary processes for the Cretaceous orogeny in the Alps. Memorie della Societa` Geologica France 156, 345–367.
Puissant, A., Van Den Eeckhaut, M., Malet, J.P., Maquaire, O., 2014. Landslide consequence analysis: a region-scale indicator-based methodology. Landslides 11 (5), 843–858. https://doi.org/10.1007/s10346-013-0429-x.
Raspini, F., Ciampalini, A., Bianchini, S., Bardi, F., Di Traglia, F., Basile, G., Moretti, S., 2016. Updated landslide inventory of the area between the Furiano and Rosmarino creeks (Sicily, Italy). J. Maps 12 (5), 1010–1019. https://doi.org/10.1080/17445647.2015.1114975.
Raspini, F., Bianchini, S., Ciampalini, A., Del Soldato, M., Solari, L., Novali, F., Del Conte, S., Rucci, A., Ferretti, A., Casagli, N., 2018. Continuous, semi-automatic monitoring of ground deformation using Sentinel-1 satellites. Sci. Rep. 8 (1), 7253. https://doi.org/10.1038/s41598-018-25369-w.
Ratto, S., Bonetto, F., Comoglio, C., 2003. The October 2000 flooding in Valle d'Aosta (Italy): event description and land planning measures for the risk mitigation. Int. J. River Basin Manag. 1 (2), 105–116. https://doi.org/10.1080/15715124.2003.9635197.
Rosi, A., Tofani, V., Tanteri, L., Stefanelli, C.T., Agostini, A., Catani, F., Casagli, N., 2018. The new landslide inventory of Tuscany (Italy) updated with PS-InSAR: geomorphological features and landslide distribution. Landslides 15 (1), 5–19. https://doi.org/10.1007/s10346-017-0861-4.
Salvatici, T., Tofani, V., Rossi, G., D'Ambrosio, M., Stefanelli, C.T., Masi, E.B., Rosi, A., Pazzi, V., Vannocci, P., Petrolo, M., Catani, F., Ratto, S., Stevenin, H., Casagli, N., 2018. Application of a physically based model to forecast shallow landslides at a regional scale. Nat. Hazards Earth Syst. Sci. 18 (7), 1919–1935. https://doi.org/10.5194/nhess-18-1919-2018.
Sartori, M., 1987. Structure de la Zone du Combin entre le Diablons et Zermatt. Eclogae Geol. Helv. 80, 789–814.
Schwendtner, B., Papathoma-Köhle, M., Glade, T., 2013. Risk evolution: how can changes in the built environment influence the potential loss of natural hazards? Nat. Hazards

Earth Syst. Sci. 13 (9), 2195–2207. https://doi.org/10.5194/nhess-13-2195-2013.
Solari, L., Barra, A., Herrera, G., Bianchini, S., Monserrat, O., Béjar-Pizarro, M., Crosetto, M., Sarro, R., Moretti, S., 2018. Fast detection of ground motions on vulnerable elements using Sentinel-1 InSAR data. Geomat. Nat. Hazards Risk 9 (1), 152–174. https://doi.org/10.1080/19475705.2017.1413013.
Solari, L., Del Soldato, M., Montalti, R., Bianchini, S., Raspini, F., Thuegaz, P., Bertolo, D., Tofani, V., Casagli, N., 2019. A Sentinel-1 based hot-spot analysis: landslide mapping in north-western Italy. Int. J. Remote Sens. 1–24. https://doi.org/10.1080/01431161.2019.1607612.
Sterlacchini, S., Akbas, S.O., Blahut, J., Mavrouli, O.C., Garcia, C., Luna, B.Q., Corominas, J., 2014. Methods for the characterization of the vulnerability of elements at risk. Mountain Risks: From Prediction to Management and Governance. Springer, Dordrecht, pp. 233–273.
Strozzi, T., Farina, P., Corsini, A., Ambrosi, C., Thüring, M., Zilger, J., Wiesmann, A., Wegmüller, U., Werner, C., 2005. Survey and monitoring of landslide displacements by means of L-band satellite SAR interferometry. Landslides 2 (3), 193–201. https://doi.org/10.1007/s10346-005-0003-2.
Strozzi, T., Ambrosi, C., Raetzo, H., 2013. Interpretation of aerial photographs and satellite SAR interferometry for the inventory of landslides. Remote Sens. (Basel) 5 (5), 2554–2570. https://doi.org/10.3390/rs5052554.
Takahashi, T., Nakagawa, H., Harada, T., Yamashiki, Y., 1992. Routing debris flows with particle segregation. J. Hydraul. Eng. 118 (11), 1490–1507. https://doi.org/10.1061/(asce)0733-9429(1992)118:11(1490).
Tomás, R., Pagán, J.I., Navarro, J.A., Cano, M., Pastor Navarro, J.L., Riquelme, A., Cuevas-González, M., Crosetto, M., Barra, A., Monserrat, O., Lopez-Sanchez, J.M., et al., 2019. Semi-automatic identification and pre-screening of geological–Geotechnical deformational processes using persistent scatterer interferometry datasets. Remote Sens. (Basel) 11 (14), 1675. https://doi.org/10.3390/rs11141675.
Trigila, A., Iadanza, C., Spizzichino, D., 2010. Quality assessment of the Italian landslide inventory using GIS processing. Landslides 7 (4), 455–470. https://doi.org/10.1007/s10346-010-0213-0.
Uzielli, M., Nadim, F., Lacasse, S., Kaynia, A.M., 2008. A conceptual framework for quantitative estimation of physical vulnerability to landslides. Eng. Geol. 102 (3-4), 251–256. https://doi.org/10.1016/j.enggeo.2008.03.011.
Van Westen, C.J., Van Asch, T.W., Soeters, R., 2006. Landslide hazard and risk zonation—why is it still so difficult? Bull. Eng. Geol. Environ. 65 (2), 167–184. https://doi.org/10.1007/s10064-005-0023-0.
Vranken, L., Van Turnhout, P., Van Den Eeckhaut, M., Vandekerckhove, L., Poesen, J., 2013. Economic valuation of landslide damage in hilly regions: a case study from Flanders. Belgium. Sci Total Environ 447, 323–333.
Wichmann, V., Heckmann, T., Haas, F., Becht, M., 2009. A new modelling approach to delineate the spatial extent of alpine sediment cascades. Geomorphology 111 (1-2), 70–78. https://doi.org/10.1016/j.geomorph.2008.04.028.
Wichmann, V., 2017. The Gravitational process Path (GPP) model (v1. 0)–a GIS-based simulation framework for gravitational processes. Geosci. Model. Dev. 10 (9). https://doi.org/10.5194/gmd-2017-5.
Winter, M.G., Smith, J.T., Fotopoulou, S., Pitilakis, K., Mavrouli, O., Corominas, J., Argyroudis, S., 2014. An expert judgement approach to determining the physical vulnerability of roads to debris flow. Bull. Eng. Geol. Environ. 73 (2), 291–305. https://doi.org/10.1007/s10064-014-0570-3.
Zimmermann, M., Mani, P., Gamma, P., Gsteiger, P., Heiniger, O., Hunziker, G., 1997. Murganggefahr und Klimaänderung-ein GIS-basierter Ansatz [debris flow risk and climatic change–a GIS-based approach]. Zürich, vdf Hochschulverlag AG an der ETH Zürich, Switzerland.